WIS-91/43/July-PH

Ionisation of H Rydberg atoms: Fractals and powerlaw decay

by

C. F. Hillermeier
Max-Planck-Institut für Quantenoptik, W-8046 Garching, Germany
R. Blümel*)
Dept. of Chemistry, Univ. of Pennsylvania, Philadelphia, PA 19104-6323, USA
and
U. Smilansky**)
H. H. Wills Physics Laboratory, Bristol, BS8 1TL, England

Abstract

Concepts from the theory of transient chaos are applied to study the classical ionization process of a one-dimensional model of kicked hydrogen Rydberg atoms. The phase-space dynamics is represented by a mapping T which is proved to be hyperbolic. The fraction of atoms not ionized after time t, $P_B(t)$, decays asymptotically according to $P_B(t) \sim t^{-\alpha}$ with $\alpha \approx 1.65$. The observed algebraic decay, which seems to contradict the hyperbolicity of T, is explained by (i) the symbolic dynamics of T consists of a countably infinite number of symbols and (ii) the invariant manifold of phase-space points which never ionize is an anomalously scaling fractal. Therefore, the one-dimensional kicked hydrogen atom provides a counterexample to the hypothesis that algebraic decay marks regular dynamics, whereas hyperbolic systems decay exponentially. The algebraic decay is reproduced by an analytically solvable diffusion model which predicts $\alpha = 3/2$. Replacing zero-width δ-kicks by smooth finite-width pulses, the mapping T is no longer completely hyperbolic, and a subset of phase-space is regular. For this case we observe that $P_B(t)$ shows a transition between two power-law decays with $\alpha \approx 1.65$ for short times and $\alpha \approx 2.1$ for long times where the effect of the regular domains is felt.

PACS: 05.45.+b; 32.80.Rm

*) Heisenberg fellow of the Deutsche Forschungsgemeinschaft
**) Permanent address: Dept. of Nuclear Physics, The Weizmann Institute, 76100 Rehovot, Israel

51 pages

1. Introduction

Fractal sets[1-3] appear most naturally in dynamical systems whenever there exists a mechanism which eliminates phase-space points from the region of interest. Fractal sets were first encountered in dissipative systems[4,5]. The dissipation is responsible for the shrinking of the originally occupied phase-space to a set of measure zero (the attractor) which, for nontrivial cases, is a fractal set[5]. In nondissipative (Hamiltonian) dynamics, fractal functions appear when phase-space points may leak away as, e.g., in scattering[6-9], ionization[10,11], or spontaneous decay[12,13].

In the present paper we shall study a system which is ionized due to an external force which is applied to it periodically. To gain some insight into the classical ionization process, consider a set S of phase-space points. To each point $s \epsilon S$ we assign a life time $L(s)$ which is the number of field cycles needed to promote the point to the continuum. If the dynamics of the system is chaotic, $L(s)$ will be a fractal function on S [6-11]. This behavior can be understood qualitatively by investigating the life-time function $L(s)$ for a special choice of the set S namely a segment of a line in phase-space. Many physical systems of interest can be modelled by a driving force which removes a fraction g of the points in S after the first period, leaving k separated intervals in S with a life time L longer than 1. After the next period of the field, the same fraction g is removed, and k new intervals replace each old interval. When this process is repeated *ad infinitum*, one obtains a life-time function which is singular on the Cantor set of phase-space points whose life time is infinite. (The canonical Cantor set[14-16], the "middle-third set", is obtained for $g = 1/3, k = 2$). It is clear that the Lebesgue measure of the set of points which are not removed after N iterations depends exponentially on N, namely, $P_B(N) = e^{-N|\ln(1-g)|}$. A second characteristic consequence of an iterative application of a time-independent depletion rule of the type above is that the resulting set is a scaling fractal which therefore can be described by the mathematical concept of a fractal dimension[1-3,17].

Hamiltonian systems can be divided into two classes: strongly chaotic (hyperbolic) systems and systems with a mixed phase space. The process of depletion of the type described above belongs to the realm of strongly chaotic systems and is exemplified by Smale's horseshoe mechanism[18,19]. Realizations of Smale's model are well known in chaotic scattering theory[6,7,9], where Smale's mechanism leads to an exponential decay of phase-space population[20,21]. This results in a depletion of all phase-space points except for a fractal set, the "invariant set" which consists of all the trapped orbits of the system. On the other

hand, most Hamiltonian systems which ionize by an external field are examples of decaying systems with a mixed phase space[10,11]. Typically, there remains a rest-population of nonzero Lebesgue-measure due to finite islands of stability, which are surrounded by unbroken KAM surfaces.

Apart from an exponential decay of ensemble populations and a decay which leads to a rest-population of finite Lebesgue-measure, there is a third type of decay which leaves a rest-population of zero Lebesgue-measure but is nevertheless characterized by an algebraic decay of phase-space populations[22]. Formally, a decay of this type can be produced by the fractal generating process described in Ref. 23. It is an explicitly time dependent modification of Cantor's middle third rule. At every time step $N \geq 1$ one has to take out not the middle third of the rest intervals, but the middle $\frac{1}{3N}$. For large N this fractal generating mechanism leads to a power-law decay of the *unit interval*[23,24]. We have $P_B(N+1) = (1 - \frac{1}{3N})P_B(N)$ which, for large N, results in the asymptotic decay law $P_B(N) \sim N^{-\alpha}$ with $\alpha = 1/3$. Applying to the resulting invariant set the usual definition of the fractal dimension d_0 yields $d_0 = 1$. This can be reconciled with the zero linear extent of the invariant set by noting that, as a consequence of the explicit time dependence of the fractal generating mechanism, the scaling symmetry of the fractal set under consideration is broken. Therefore, the characterization of the fractal by d_0 alone is incomplete. It has to be completed by additional dimensions d_ν allowing for the decay to result in a rest population of zero Lebesgue-measure[23] (see section 5).

The question arises whether a fractal generating mechanism accompanied by a power-law decay can also be found in physical Hamiltonian systems. In other words, we ask the question whether Hamiltonian systems exist, which satisfy the following three conditions: (i) the dynamical evolution is completely chaotic inside a region S of phase-space, (ii) S decays according to a power-law in time, and (iii) the rest population in S is of measure zero. The conditions (i) and (ii) seem to contradict each other. In fact, there is evidence for the hypothesis that power-law decay is attributed to systems whose dynamics is regular, and exponential decay to systems with chaotic dynamics[13]. This assignment, however, cannot be one-to-one. When phase-space has both regular and chaotic regions, particles initialized in a chaotic region (and as a consequence dynamically restricted to the chaotic region for all times) can "stick" a long time to the vicinity of the boundary of a regular region. In many cases, the leaking away of particles from sticky boundaries will give an algebraic decay, as can be concluded from numerical simulations[25,26] and from a model of

Hamiltonian transport theory[27-29].

In the following, we shall present an even stronger counterexample to the suggested assignment of algebraic decay to regular dynamics and of exponential decay to chaotic dynamics. We will present a hyperbolic system (no regular regions in phase-space) which satisfies the conditions (i) – (iii). Furthermore, we will show that the conditions (*i*) and (*ii*) are consistent if the system is described by a symbolic dynamics with an infinite number of symbols.

Our model consists of a one-dimensional hydrogen Rydberg atom[30-38] subjected to a train of strong microwave pulses of zero width. In this case, the dynamical evolution can be described by a simple analytical mapping[39,40], which is proved to be hyperbolic. According to a widely accepted working hypothesis in chaotic scattering[6-9], one should therefore expect an exponential decay of phase-space ensembles[20,21,24]. For a Rydberg electron whose initial condition is drawn randomly out of a classical microcanonical ensemble[41], we will show, however, that the survival probability, $P_B(N)$, i.e., the probability that the electron is still bound to the atom after N cycles of the external field, decays as a power of N when perturbed by a sequence of δ-kicks: $P_B(N) \sim N^{-\alpha}$ with $\alpha \approx 1.65$.

To investigate this decay phenomenon, we adopt two types of approach: As long as our interest in the dynamics of a microcanonical ensemble is focussed on its Lebesgue-measure as a function of time, a stochastic description is in order. Within this framework, the existence of the asymptotic power-law and the scaling of the decay-curves with the initial energy and the kick strength can be explained with the help of an analytically solvable model of a random-walk in phase-space. The second approach employs the tools provided by the theory of transient chaos[9] and chaotic scattering[6-9] in order to study the structure of the life-time function which assigns to each individual phase-space point of the microcanonical distribution its characteristic life time L. We will show that the singularities of the life time function form a phase-space fractal with broken scaling symmetry which underlies the power-law decay of the ensemble.

We should emphasize that unlike the modified Cantor process[23] discussed briefly above, the fractal generating mechanism for the description of ionization in our model is not an externally imposed rule which depends explicitly on the "iteration step" N of the fractal generating process or, equivalently, the sequence number N of the microwave pulses. On the contrary, in our model the breaking of the scaling symmetry is generated by the nonlinear dynamics itself. This result, like the consistency of the conditions (i) and (ii),

rests on the fact that our system is described by a symbolic dynamics with a (countably) infinite alphabet.

The paper is organized as follows: In section 2 we present the physical model and derive the mathematical mapping which describes the dynamical evolution of our system. We shall present two proofs for the hyperbolicity of T. The first is algebraic and specially taylored to the system at hand. The second is more general and applicable to a whole class of hyperbolic Poincaré mappings. Section 3 provides numerical evidence for the power-law decay of a microcanonical ensemble of initial conditions and discusses the stochastic model for this decay process. A thorough treatment of the fractal fluctuations of the life time function follows in section 4. The time independence of the fractal generating rule is shown by establishing a symbolic description of the dynamics which enables us to state the fractal generating rule explicitly. In section 5 we review briefly the mathematics of fractal sets with broken scaling symmetry and calculate explicitly the first logarithmic correction to the fractal dimension of the hydrogen fractal. In section 6 we extend our model to microwave pulses of finite width and demonstrate the existence of a transition between two powerlaw regimes. The paper will be summarized and concluded in section 7.

2. The Model

The starting point of our discussion is the classical one-dimensional model of a periodically kicked hydrogen Rydberg-atom[39,40]:

$$H = H_0 - \beta\, x\, \delta_{2\pi}(\omega t) \tag{2.1a}$$

$$H_0(x,p) = \begin{cases} \frac{p^2}{2} - \frac{1}{x} & \text{for } x > 0 \\ \infty & \text{for } x \leq 0 \end{cases} , \tag{2.1b}$$

where β is the kick-strength, ω the kick-frequency and $\delta_{2\pi}$ is the 2π - periodic δ-function. With respect to H_0, phase-space is naturally divided into two disjoint subspaces, the bounded space and the continuum. Points in the bounded space, (x_B, p_B), are characterized by a negative energy, $H_0(x_B, p_B) < 0$, whereas a point (x_C, p_C) in the continuum satisfies $H_0(x_C, p_C) > 0$. In the bounded space, the equations of motion for H_0 are solved by a canonical transformation to action-angle variables[30-35]:

$$H_0 = -\frac{1}{2\nu^2}; \quad \Theta = 2\eta - \sin(2\eta)$$

$$x = 2\nu^2 \sin^2(\eta); \quad p = \frac{1}{\nu}\cot(\eta) \quad . \tag{2.2}$$

The equations of motion for ν and Θ under the action of H defined in (2.1a) are given by

$$\dot{\nu} \;=\; -\frac{\partial H}{\partial \Theta} \;=\; \beta\,\delta_{2\pi}(\omega t)\,\nu^2\,\cot(\eta)$$

$$\dot{\Theta} \;=\; \frac{\partial H}{\partial \nu} \;=\; \frac{1}{\nu^3} \;-\; 4\,\nu\,\beta\,\sin^2(\eta)\,\delta_{2\pi}(\omega t) \quad . \tag{2.3}$$

The equations of motion (2.3) are invariant under the scale transformation $\nu \to \bar{\nu} = \nu/\nu_0$ provided that frequency, interaction strength and time are scaled according to[41]

$$\omega \to \omega_0 \;=\; \omega\,\nu_0^3\,; \quad \beta \to \beta_0 \;=\; \beta\,\nu_0^4\,; \quad t \to t_0 \;=\; t/\nu_0^3 \quad . \tag{2.4}$$

Exploiting the invariance of (2.3) under (2.4) it is advantageous to introduce the scaled action

$$n \;=\; \beta\,\nu\,/\,\omega \tag{2.5}$$

and the control parameter

$$\xi \;=\; \beta^3\,/\,\omega^4 \quad . \tag{2.6}$$

Both quantities are invariant under the Coulomb scale-transformation (2.4). Defining the scaled time

$$\tau \;=\; \xi\,\omega\,t \quad , \tag{2.7}$$

the following set of equations of motion for the scaled action n and the angle Θ can be derived from (2.3):

$$\frac{dn}{d\tau} \;=\; \frac{1}{\xi}\,n^2\,\cot(\eta)\,\delta_{2\pi}(\tau/\xi)$$

$$\frac{d\Theta}{d\tau} \;=\; \frac{1}{n^3} \;-\; \frac{4n}{\xi}\,\sin^2(\eta)\,\delta_{2\pi}(\tau/\xi) \quad . \tag{2.8}$$

Alternatively, the equations of motion (2.8) can be derived directly from the scaled Hamiltonian

$$\tilde{H} \;=\; H_0(\tilde{x},\tilde{p}) \;-\; \frac{1}{\xi}\,\tilde{x}\,\delta_{2\pi}(\tau/\xi) \tag{2.9}$$

where the scaled position and momentum is constructed with the help of the scaled action (2.5) from (2.2) according to

$$\tilde{x} \;=\; 2n^2\,\sin^2\eta\,; \quad \tilde{p} \;=\; \frac{1}{n}\,\cot\eta \quad . \tag{2.10}$$

In action-angle variables, and restricted to the bounded space, the Hamiltonian (2.9) is then given by

$$\tilde{H} \;=\; -\frac{1}{2n^2} \;-\; \frac{1}{\xi}\,2n^2\,\sin^2(\eta)\,\delta_{2\pi}(\tau/\xi) \quad . \tag{2.11}$$

The time-evolution of a phase-space point (Θ, n) over one cycle of the external perturbation is conveniently represented in the form of an area-preserving mapping

$$T: \ (\Theta, n) \rightarrow (\Theta'', n'') \quad . \tag{2.12}$$

The mapping is constructed in four steps[39,40]:

(i) Transformation of (Θ, n) to $(\bar{x}, \bar{p})$ via (2.10).

(ii) Kick:

$$\bar{x}' \ = \ \bar{x}; \ \ \bar{p}' \ = \ \bar{p} \ + \ 1 \quad . \tag{2.13}$$

Increasing the momentum via (2.13) can promote the Rydberg electron to the continuum. In order to check whether the electron is still bounded after the application of a kick, the energy after the kick, E', has to be evaluated:

$$E' \ = \ E \ + \ \bar{p} \ + \ 1/2 \quad . \tag{2.14}$$

For $E' < 0$ the electron is still bounded and we can proceed with step (iii) of the mapping. For $E' > 0$ the electron is called ionized. Two cases have to be distingished. For $\xi < 0$ it is possible that the ionized electron re-enters the bounded space ($E < 0$) at some future time τ_R. For $\xi > 0$ the momentum of an electron immediately after the ionizing kick is positive ($\bar{p}' > 1/2$) and according to (2.14) the energy of the electron increases monotonically from there on. This means that an ionized electron is never again trapped back into the $E < 0$ region and therefore stays ionized forever. This simplification is the reason why we will concentrate exclusively on the case $\xi > 0$ in the sequel.

(iii) Transformation of $(\bar{x}', \bar{p}')$ back to (Θ', n') via (2.10).

(iv) Free motion:

$$n'' \ = \ n'; \quad \Theta'' \ = \Theta' + \xi \, \frac{2\pi}{n'^3} \quad . \tag{2.15}$$

The mapping T can be decomposed into a "kick" and a "twist" according to

$$T \ = \ T_{twist} \circ T_{kick} \quad . \tag{2.16}$$

The name "twist" for the free propagation over one kick-period is used because it corresponds to a rotation on the phase-space cylinder if $\Theta = 0$ and $\Theta = 2\pi$ are identified. The kick-mapping is given by:

$$T_{kick}: \ \begin{cases} n' = \frac{n}{\sqrt{1 - 2n\cot\eta - n^2}} \ = \ n \, \frac{\sin\eta}{\sin\eta'} \\ \eta' \ = \ \begin{cases} \arcsin\{\sin(\eta)[1 - 2n\cot(\eta) - n^2]^{1/2}\} & \text{for } p' > 0 \\ \pi - \arcsin\{\sin(\eta)[1 - 2n\cot(\eta) - n^2]^{1/2}\} & \text{for } p' < 0 \end{cases} \end{cases} \quad . \tag{2.17}$$

The twist-mapping is given by (2.15), i.e.,

$$T_{twist}: \begin{cases} n'' &= n' \\ \Theta'' &= \Theta' + \xi \frac{2\pi}{n'^3} \end{cases} . \tag{2.18}$$

Thus, the classical one-cycle propagator for the one-dimensional model of the kicked hydrogen atom forms a one-parameter family of mappings.

The domain of T in the (Θ, E) phase-space consists of all points with $E < 0$ which are still bound after one application of T. This set will be denoted by I^{-1}. Since the domain of T_{twist} is the unrestricted (Θ, E) phase-space, the domain I^{-1} of the mapping T is identical with the domain I^{-1}_{kick} of T_{kick}, where I^{-1}_{kick} is given by

$$n = \left(\frac{1}{2|E|}\right)^{1/2} < \tan(\eta(\Theta)/2) . \tag{2.19}$$

The domain I^{-1} of T is shown as the shaded area in Fig. 1a. Also shown in Fig. 1a is the intersection of I^{-1} with a $n = 1 = const.$-line. The straight line in Fig. 1a (the thick black line) actually consists of 200 equi-distantly placed phase-space points which are mapped under the action of T into the discrete points shown in Fig. 1b. The image of I^{-1} is also shown in Fig. 1b. It consists of a system of stripes (shaded areas in Fig. 1b) which will be the focus of attention in section 4.

All points $p \in I^{-1}$ are linearly unstable. This is shown in the following way. Since for $p \in I^{-1}$ all four steps (i)-(iv) of the mapping T are defined, the Jacobian of the mapping T, $J = (\partial\Theta'' n''/\partial\Theta n)$, can be calculated as the product of the four Jacobians corresponding to the four steps of the mapping, i.e., $J = J_4 \cdot J_3 \cdot J_2 \cdot J_1$ with $J_1 = \left(\frac{\partial \tilde{x}\tilde{p}}{\partial\Theta n}\right)$, $J_2 = \left(\frac{\partial \tilde{x}'\tilde{p}'}{\partial \tilde{x}\tilde{p}}\right)$, $J_3 = \left(\frac{\partial\Theta' n'}{\partial \tilde{x}'\tilde{p}'}\right)$, $J_4 = \left(\frac{\partial\Theta'' n''}{\partial\Theta' n'}\right)$. Since $I_2 = 1$ and $J_3 = J_1^{-1}$ evaluated at the "primed" coordinates, we need only

$$J_1 = \begin{pmatrix} n^3\tilde{p} & 2\tilde{x}/n \\ -n^3/\tilde{x}^2 & -\tilde{p}/n \end{pmatrix} ; \quad J_4 = \begin{pmatrix} 1 & -6\pi\xi/n'^4 \\ 0 & 1 \end{pmatrix} \tag{2.20}$$

to calculate

$$J = \begin{pmatrix} \frac{r}{2}[1 + r^2 + n^2] + \frac{6\pi\xi r n^2}{\tilde{x}^2} & -\frac{2\tilde{x}}{nn'} - \frac{3\pi\xi}{n'^3}[1 + r^2 + n^2] \\ -\frac{(nn')^3}{\tilde{x}^2} & \frac{1}{2r^3}[1 + r^2 + n^2] \end{pmatrix} . \tag{2.21}$$

We defined $r = n/n'$. Since T represents the one-cycle dynamics of a Hamiltonian system, we have det J=1. The trace of J is given by

$$TrJ = \frac{1}{2}(r^2 + \frac{1}{r^2})(r + \frac{1}{r} + nn') + \frac{6\pi\xi r n^2}{\tilde{x}^3} . \tag{2.22}$$

For $\xi > 0$ we have immediately $TrJ > \frac{1}{2}(r^2 + \frac{1}{r^2})(r + \frac{1}{r})$, and since in general $\lambda + 1/\lambda > 2$ for all $\lambda > 0$, we have $TrJ > 2$. This means that J has real eigenvalues and therefore all points $p \in I^{-1}$ are linearly unstable[18]. In particular this implies that all period-1 fixed points of T are unstable. This observation, however, is not enough to ascertain the hyperbolicity of the mapping T. In order for T to be hyperbolic, all fixed points of $T^N, N = 1, 2, \ldots$ must be unstable. In order to prove the hyperbolicity of T, we note that the Jacobian (2.21) is of the form

$$J = \begin{pmatrix} \frac{r^2}{2}[r + 1/r + \epsilon] + A & -B \\ -C & \frac{1}{2r^2}[r + 1/r + \epsilon] + D \end{pmatrix} \tag{2.23}$$

with $A, B, C, D, \epsilon \geq 0$ for $\xi > 0$. In order to calculate the Jacobian $J^{(N)}$ of T^N, we have to form products of Jacobians with the structure (2.23) evaluated at the intermediate image points of the iterated mapping T. Consider the product of two Jacobians $J' = \tilde{J} \cdot \bar{J}$ evaluated at arbitrary coordinates $\tilde{x}, \tilde{p}$ and $\bar{x}, \bar{p}$, respectively. We obtain:

$$J' = \begin{pmatrix} \frac{(\tilde{r}\bar{r})^2}{4}(\tilde{r} + 1/\tilde{r} + \tilde{\epsilon})(\bar{r} + 1/\bar{r} + \bar{\epsilon}) + A' & -B' \\ -C' & \frac{1}{4(\tilde{r}\bar{r})^2}(\tilde{r} + 1/\tilde{r} + \tilde{\epsilon})(\bar{r} + 1/\bar{r} + \bar{\epsilon}) + D' \end{pmatrix} \tag{2.24}$$

with $A', B', C', D', \epsilon' \geq 0$. In the same way, the Jacobian of T^N is given by

$$J^{(N)} = \begin{pmatrix} \frac{1}{2^N}\prod_{j=1}^{N} r_j^2 (r_j + 1/r_j + \epsilon_j) + A^{(N)} & -B^{(N)} \\ -C^{(N)} & \frac{1}{2^N}\prod_{j=1}^{N} \frac{1}{r_j^2}(r_j + 1/r_j + \epsilon_j) + D^{(N)} \end{pmatrix} \tag{2.25}$$

with $\epsilon_j > 0, j = 1, 2, \ldots N$, and $A^{(N)}, B^{(N)}, C^{(N)}, D^{(N)} > 0$. With (2.25) it is trivial to get an estimate for the trace of $J^{(N)}$. In fact:

$$\begin{aligned} TrJ^{(N)} &> \frac{1}{2^N}\left(\prod_{j=1}^{N} r_j^2 (r_j + 1/r_j) + \prod_{j=1}^{N} \frac{1}{r_j^2}(r_j + 1/r_j)\right) \\ &> \prod_{j=1}^{N} r_j^2 + \frac{1}{\prod_{j=1}^{N} r_j^2} > 2 \quad . \end{aligned} \tag{2.26}$$

Thus we proved that T defined in (2.16) – (2.18) is indeed hyperbolic. We emphasize that this property holds only in the case of positive kicks, i.e., $\xi > 0$. Mappings corresponding to negative kicks or kicks whose strengths alternate in time[42,43] are not hyperbolic. They exhibit a mixed phase-space with intermingled regular and chaotic regions.

A more intuitive prove of the hyperbolicity of T is presented in Ref. 44. Suppose that R is a fixed point of the mapping T^N and Q is a point infinitely close by. If the

fixed point R were elliptic, the slope of the straight line segment connecting the points $Q^{(M)} = T^{M \cdot N}(Q)$ and R has to change sign as $\overline{Q^{(M)}R}$ rotates around R under successive applications of T^N. In Ref. 44, however, it is shown that T^N maps a monotonically falling curve of infinitesimal length into a monotonically falling curve for any N. Therefore, R cannot be elliptic. This proof of hyperbolicity is generally applicable to the whole class of Poincaré-mappings which conserve in a similar way the monotony of curves. To reveal such a conservation-feature for a given Poincaré-mapping may require a suitable canonical transformation of the coordinates.

The proof which is based on the monotony-conservation of T allows for a corollary: For any (hyperbolic) fixed point R of the mapping T^N the stable eigenvector has to have a positive slope in (θ, n)-phase-space, whereas the unstable eigenvector has a negative slope. This feature can be considered a generalisation of Smale's horseshoe model, where one stable and one unstable direction are universal for all periodic points.

3. Powerlaw decay

When a *microcanonical* ensemble of initial conditions[41] is exposed to a train of δ-kick pulses, the set of phase-space points which remains bounded decays with the number of kick-pulses according to a powerlaw. This unexpected feature is illustrated in Fig. 2. It displays several decay curves resulting from the repetitive application of the mapping T with $\xi = 1$ to five initial straight-line ensembles with $n_0 = 1.0, 0.5, 0.25, 0.1, 0.05$ and Θ drawn randomly and uniformly from $[0, 2\pi]$. Straight-line ensembles were chosen as initial conditions since they are the closest classical approximation to a quantum mechanical eigenstate of (2.1b). In the sequel we shall use the abbreviation MCE for microcanonical ensemble. The long-time asymptotics of the classical decay curves displayed in Fig. 2 clearly show an algebraic decay. The value of the power extracted from the numerical data, $\alpha \approx 1.65$, was found to be independent of the initial energy E_0 and of the control parameter ξ if $\xi \gtrsim 1$. The consequences of the powerlaw for the fractal properties of the invariant set of the mapping T are addressed in sections 4 and 5. In this section we will clarify its dynamical origin by means of a random-walk model. We approximate the deterministic dynamics described by the mapping T by a nontrivial random-walk in one dimension, the energy E. Not only does this model elucidate the dynamical process responsible for the powerlaw, but predicts scaling properties of the decay curves which are obeyed by the numerical data of the deterministic mapping to a high degree of accuracy.

Let us follow the time evolution of a MCE at $E = E_0$. With (2.2), (2.14) and (2.17)

it is easy to calculate the probability distribution $\rho_{E_0}(E')$ of energies E' after a kick was applied to the ensemble at $E = E_0$. The probability distribution of momenta, $\rho(\bar{p})$, of a MCE satisfies $\rho(\bar{p})d\bar{p} = \rho(\Theta)d\Theta = d\Theta/2\pi$, from which we get $\rho(\bar{p}) = 2n_0 \sin^4(\eta)/\pi = 2n_0 \sin^4[\text{arccot}(n_0\bar{p})]/\pi = (2n_0/\pi)/[(n_0\bar{p})^2 + 1]^2$. Because of (2.14), $\rho(\bar{p})d\bar{p} = \rho(E')dE'$ and finally:

$$\rho_{E_0}(E') = \frac{\sqrt{2}}{\pi\sqrt{|E_0|}\left[1 + \frac{1}{2|E_0|}\left(E' - E_0 - \frac{1}{2}\right)^2\right]^2} \quad . \tag{3.1}$$

While $\rho_{E_0}(E')$ remains unaltered by the subsequent twist, the image of the MCE after one kick is wrapped around the (Θ, E) - cylinder infinitely often owing to the singularity of the Kepler-frequency $\frac{1}{n^3}$ in the twist-mapping (2.18) (see Fig. 1b). Thus, the unperturbed motion between two kicks has a strongly randomizing effect on the angle variable of the image points. Having propagated the MCE over one kick-period, we end up with a set of almost horizontal lines in (Θ, E)-space, covered with an almost homogeneous point density (see Fig. 1b). This implies, that the time evolution over the next kick-period can be approximated by assuming that each of the lines is itself a MCE, and by disregarding memory effects in the Θ distribution.

The absence of memory effects was checked by comparing the energy distributions $\rho^{(T)}(E)$ and $\rho^{(R\circ T)}(E)$ for the exact mapping T and the composite mapping $R \circ T$, respectively, where R randomizes the phases according to $R(\Theta, E) = (\bar{\Theta}, E)$, $\bar{\Theta}$ uniformly random in $[0, 2\pi]$. For $n_0 = 0.2$ and $\xi = 1$ we compared $\rho^{(T)}(E)$ and $\rho^{(R\circ T)}(E)$ for $N = 1, 2, ..., 12$ applications of the respective mappings and found the two distributions to be indistinguishable. This proves that phase-memory is not important for the mapping T. In another test, we checked the idea that phase-space points in a band $E_1 - \Delta \leq E \leq E_1 + \Delta$ can effectively be represented by an MCE at $E = E_1$ with uniformly distributed angles. To this effect, we propagated a straight-line ensemble started at $n_0 = 0.25$ over ten kick-periods with $\xi = 1$. All points arriving in $E_1 - \Delta \leq E \leq E_1 + \Delta$, $E_1 = -2.0, \Delta = 0.2$, were exposed to another kick to obtain $\rho(E)$. Subsequently, a MCE at E_1 was propagated over one kick to obtain $\bar{\rho}(E)$. Both $\rho(E)$ and $\bar{\rho}(E)$ turned out to be practically identical within the statistical errors.

Thus, we arrive at the following Markovian random-walk in energy as a model for the underlying deterministic evolution of a MCE: For any momentary energy-position E, the energy-position E' after one more kick-cycle is drawn randomly out of an ensemble with a probability distribution given by $\rho_E(E')$.

In the following we will derive an analytical expression for the time-evolution of this energy-distribution — more precisely, of the leaking out of the energy-distribution into the continuum — on the basis of the Markovian model. The present random-walk occurs in discrete time steps of size $2\pi\xi$. It is characterized by a constant drift-term $\frac{1}{2}$ and a stochastic increment ΔE_{stoch} , whose probability distribution $\tilde{\rho}_E(\Delta E_{stoch})$ depends on the energy-position E and is closely related to $\rho_E(E')$ by

$$\tilde{\rho}_E(\Delta E_{stoch}) \;=\; \rho_E\left(E_0 + \frac{1}{2} + \Delta E_{stoch}\right) \;=\; \frac{\sqrt{2}}{\pi\sqrt{|E|}\left[1 \;+\; \frac{1}{2|E|}\left(\Delta E_{stoch}\right)^2\right]^2} \quad . \tag{3.2}$$

The variance of the stochastic increment caused by the next kick-pulse is proportional to the current energy-position and explicitly given by

$$< (\Delta E_{stoch})^2 > = \; 2\,|E| \quad . \tag{3.3}$$

If the stochastic increment were exactly that of a Wiener Process[45], i.e., drawn from a probability distribution of Gaussian shape, one could regard the present random-walk as the discrete-time approximation of a random walk continuous in time, which can be described by a Fokker-Planck equation[45]. In order to avoid the difficulties of dealing with colored noise in the continuous-time description of our stochastic process, we will proceed by approximating our random-walk problem by a suitable Wiener-process. In this spirit we replace $\tilde{\rho}_E(\Delta E_{stoch})$ by a Gaussian distribution of the same variance. This approximation is justified because of the similar shape of both probability distributions, but has a noticeable effect on the leaking out into the continuum, which will be discussed later. Based on these approximations, we obtain the following Fokker-Planck equation for the time-dependent probability distribution $f(E,\tau)$:

$$\frac{\partial f(E,\tau)}{\partial \tau} \;=\; -\frac{1}{4\pi\xi}\frac{\partial f(E,\tau)}{\partial E} \;+\; \frac{1}{2\pi\xi}\frac{\partial^2}{\partial E^2}\left((-E)f(E,\tau)\right) \quad . \tag{3.4}$$

It has to be solved together with the boundary conditions

$$f(E,\tau)|_{\tau=0} \;=\; \delta(E - E_0) \quad , \tag{3.5a}$$

$$f(E,\tau)|_{E=0} \;=\; 0 \quad . \tag{3.5b}$$

Here, the δ-shaped initial distribution (3.5a) reflects the starting microcanonical ensemble, whereas the absorbing barrier at $E = 0$ expresses the fact that positive kicks do not allow for a back-coupling from the continuum to the bound space.

Since we are only interested in the integral of $f(E,\tau)$ over all negative energies, one is confronted with the First-Passage-Time problem[45] corresponding to the Fokker-Planck equation (3.4). Starting the random-walk at energy E_0, the probability $G(E_0,\tau)$ to remain bound has to fulfill the First-Passage-Time equation[45]:

$$\frac{\partial G(E_0,\tau)}{\partial \tau} = \frac{1}{4\pi\xi}\frac{\partial G(E_0,\tau)}{\partial E_0} + \frac{1}{2\pi\xi}(-E_0)\frac{\partial^2}{\partial E_0^2}G(E_0,\tau) \quad . \tag{3.6}$$

This equation has to be solved together with the boundary conditions[45]:

$$G(E_0,\tau)|_{\tau=0} = 1 \quad \text{for } E_0 < 0 \quad , \tag{3.7a}$$

$$G(E_0,\tau)|_{E_0=0} = 0 \quad \text{for } \tau \geq 0 \quad . \tag{3.7b}$$

The condition (3.7*b*) is due to the immediate absorption of the wandering electron at the barrier $E = 0$. Since the boundary conditions require $G(E_0,\tau)$ to be constant on two straight lines through the point $E = 0, \tau = 0$, the ansatz $G(E_0,\tau) \equiv \bar{G}\left(\frac{E_0}{\tau}\right)$ appears promising. Inserting this ansatz into (3.6), one obtains an ordinary differential equation, where E_0 and τ only emerge in the combination $\frac{E_0}{\tau}$:

$$\frac{E_0}{\tau}\frac{d^2\bar{G}}{d\left(\frac{E_0}{\tau}\right)^2} = \left(\frac{1}{2} + 2\pi\xi\left(\frac{E_0}{\tau}\right)\right)\frac{d\bar{G}}{d\left(\frac{E_0}{\tau}\right)} \quad . \tag{3.8}$$

Defining $F\left(\frac{E_0}{\tau}\right) \equiv \frac{d\bar{G}\left(\frac{E_0}{\tau}\right)}{d\left(\frac{E_0}{\tau}\right)}$, we arrive at a linear homogeneous differential equation of first order, which is solved by

$$F\left(\frac{E_0}{\tau}\right) = F_0 \cdot \left|\frac{E_0}{\tau}\right|^{\frac{1}{2}} \exp\left(2\pi\xi\frac{E_0}{\tau}\right) \tag{3.9}$$

with integration constant F_0. The integral required to calculate $G(E_0,\tau)$ can be found in Ref. 46, formula 3.381. With this results, the solution of (3.6), which fulfills the boundary conditions (3.7), is given by :

$$G(E_0,\tau) = \frac{1}{\Gamma(\frac{3}{2})} \cdot \gamma\left(\frac{3}{2}, 2\pi\xi\frac{|E_0|}{\tau}\right) \quad , \tag{3.10}$$

where γ denotes the incomplete gamma function. This result can be simplified even further. Since (2.7) shows that $\tau/(2\pi\xi) = \omega t/2\pi$ is the number of kicks, N, we obtain:

$$G(E_0,N) = \frac{1}{\Gamma(\frac{3}{2})}\gamma(\frac{3}{2}, \frac{|E_0|}{N}) \quad . \tag{3.11}$$

It is astonishing that this result does not depend neither on the kick strength β nor on the kick-frequency ω. With $E_0 = -1/2n_0^2$ it is seen to be only a function of the scaled variable

$$z \;=\; 2n_0^2 N \quad . \tag{3.12}$$

Expressed in the variable z, we obtain finally:

$$G(z) \;=\; \frac{1}{\Gamma(\frac{3}{2})}\gamma(\frac{3}{2},1/z) \;=\; \mathrm{erf}(1/\sqrt{z})\;\; \frac{2}{\sqrt{\pi z}}\exp(-1/z) \quad , \tag{3.13}$$

where $\mathrm{erf}(x) \;=\; \frac{2}{\sqrt{\pi}}\int_0^x e^{-t^2}dt$ is the error function.

The scaling (3.12) is a genuine and unexpected prediction of our stochastic model. It can be checked, e.g., by properly rescaling the data presented in Fig. 2. If the scaling (3.12) were exact, the scaled P_B-data in Fig. 2 are expected to collapse onto the universal decay function $G(z)$. The function $G(z)$ is shown as the full line in Fig. 3. Also shown are survival probabilities $P_B(N)$ at selected values of N taken from Fig. 2 and scaled according to (3.12). The five different plot symbols in Fig. 3 correspond to the five different straight-line ensembles in Fig. 2, respectively. Given that the survival probabilities of the unscaled numerical data differ by a factor 5000 at $N = 200$ (see Fig. 2), the scaled data (plot symbols in Fig. 3) show that the scaling (3.12) is fulfilled to a very good degree of accuracy. The scaled data collapse within a factor 3 into a narrow band close to the theoretical prediction (3.13).

Expanding (3.13) for large arguments z, we obtain

$$G(z) \;=\; \frac{2}{3}\,z^{-3/2} \;=\; \frac{2\sqrt{2}}{3n_0^3}\,N^{-3/2}, \quad z \to \infty \quad . \tag{3.14}$$

Thus, the stochastic model confirms that the decay due to ionization follows asymptotically an algebraic law, and that the decay-power is independent of the starting energy of the microcanonical ensemble as well as of the kick-strength β and the kick-frequency ω. Moreover, the decay-power of the random-walk model, $\alpha = 3/2$, is in reasonable agreement with the decay-power extracted from the numerical data of the deterministic map, $\alpha \approx 1.65$. The reason for the discrepancy provides further insight into the dynamical mechanism which is responsible for the algebraic decay: The asymptotic power of the incomplete γ-function is given by the negative of its first argument, which in fact equals

$$\alpha = 1 + s \quad , \tag{3.15a}$$

where

$$s = \left(\frac{1}{4\pi\xi}\right) / \left(\frac{1}{2\pi\xi}\right) = \frac{1}{2} \tag{3.15b}$$

is the ratio between the constants in front of the drift-term and the diffusion-term of the Fokker-Planck-equation (3.4). Even in the absence of any drift-term, i.e., for $s = 0$, the leaking out across the absorbing barrier would follow an algebraic law, namely $\frac{1}{N}$, the slowest decay possible for a Fokker-Planck equation of the type (3.4). We learn from this consideration, that the mechanism responsible for our type of powerlaw-decay is given by the stochastic fluctuations whose variance increases linearly with $|E|$. An ever growing fraction of trajectories that are not yet ionized is wandering toward lower energy-values, thus thinning out the probability distribution near the ionization barrier at $E = 0$ and diminishing the portion of trajectories leaving the bound space per kick-period. As a result, the leaking into the continuum slows down in time and we end up not with an exponential, but with an algebraic decay. According to (3.15), the effect of the energy drift, which in our model is directed toward the absorbing barrier, is to accelerate the decay process, resulting in $\alpha = 1 + s > 1$.

Our mechanism, although very different conceptually, is nevertheless close in spirit to the mechanism discussed in Refs. 25-29. Both diffusion mechanisms lead to powerlaw decay which is explained by a progressive unavailability of trajectories for decay. But whereas trajectories in Refs. 25-29 hide from decay in a hierarchy of Cantori and stable islands, the trajectories in our model hide in phase-space regions with ever lower energy.

Because of (3.15), the actual value of the decay-power α depends quite sensitively on the drift- and diffusion-constants. This, in fact, is the main reason for the discrepancy between the powers predicted by the stochastic model and the exact calculations, respectively. In our model, $\tilde{\rho}_E(\Delta E_{stoch})$ was fitted to a Gaussian with the same variance. In order to check the effect of this approximation step, we tried an alternative fitting procedure in which the Gaussian is fitted not to the same variance but adjusted to the maximum height of the $\tilde{\rho}_E(\Delta E_{stoch})$-distribution. This choice would lead to a diffusion term of $\frac{1}{16\xi}(-E_0)$ in (3.6), i.e., to $s = \frac{4}{\pi}$. Therefore, a First-Passage-Time solution with an asymptotic decay-power of $\alpha = (1 + \frac{4}{\pi}) = 2.27$ results. Thus, the ambiguity in establishing the random-walk model has no effect on the reproduction of the powerlaw-decay itself, but does affect the exact value of the decay-power.

Concluding this section, we will now discuss some of the approximations underlying the stochastic model.

The image of a MCE consists of several "windings" (compare Fig. 1b). These windings served as secondary initial MCE's in the formulation of the stochastic model discussed above. The first of these windings, $W_{k=1}$, (the winding closest to the separatrix $E = 0$) is not well approximated by a MCE and in general tends to deteriorate the validity of the stochastic model. We can find conditions under which the effects of W_1 on the subsequent evolution can become marginal. To this end we note that only $W_1 \cap I^{-1}$ survives another application of T. Thus, the control parameter ξ has to be chosen such as to push W_1 toward the line $E = 0$. This way the surviving portion of W_1, $W_1 \cap I^{-1}$, is squeezed into the upper right corner of I^{-1} (see Fig. 1c) and only a fraction of W_1 will survive another kick. The left hand border of I^{-1} is given by $n < \tan(\eta/2)$ (see (2.19)). According to (2.18) the twist angle $2\pi\xi/n'^3$ is a sensitive function of n'. Therefore, the first winding will cut the $\Theta = 2\pi$ axis at $n' \approx \xi^{1/3}$. On the other hand, and according to Fig. 1c, n' should be larger than 1 in order to cut a large fraction of the winding W_1. Therefore, we expect that for $\xi > 1$ the influence of the first winding is negligible and the stochastic model is a good approximation. This estimate agrees with our experience based on many Monte-Carlo runs for different values of ξ. Moreover, the powerlaw tail of the survival probabilities shows most clearly for $\xi > 1$.

Another issue concerns the energy distribution function $f(E,\tau)$ of the stochastic model. The First Passage Time problem for the Fokker-Planck equation (3.4) was solved above with the boundary condition $f(E,\tau) = 0$ for $E = 0$ and all $\tau > 0$. Depending on the "draining-efficiency" of the continuum with respect to the probability flux directed toward the separatrix $E = 0$, this is indeed approximately the right boundary condition for an ionization problem with a perturbation which is bounded and continuous in time. For a perturbation consisting of a train of kicks, however, $f(E,\tau) = 0$ at $E = 0$ is not correct. This is so because of the impulsive nature of the perturbing kicks which are capable of depositing probability at $E = 0$ before the continuum gets any chance of draining this probability into the unbounded $E > 0$ portion of phase-space. That $f(E,\tau) \neq 0$ for the exact kick-dynamics is clearly exhibited by $\rho_{E_0}(E)$ which is non-zero at $E = 0$. The most straight-forward solution of the problem is obviously to replace (3.5b) with a more realistic boundary condition. This procedure, however, would almost certainly impede any attempt at solving the first passage time equation (3.6) analytically. Also, we do not believe that a somewhat inaccurate representation of $f(E,\tau)$ around $E = 0$ will change much of the physics of the problem at hand since (i) as mentioned above, $f(E,\tau) = 0$ at $E = 0$ is

the right choice for a continuous drive and (ii) phase-space points close to the continuum threshold will ionize anyway during the next kick (see the structure of the complement of I^{-1} in Fig. 1a close to $E = 0$).

4. Fractal regions of stability

When focussing on the decay features of a one-dimensional ensemble of phase-space points, a probabilistic description of the ensemble dynamics is an adequate approach as demonstrated in the previous section. Under the deterministic time evolution mediated by a sequence of T-mappings, however, each single phase-space point has a characteristic life time. To illustrate this further, let us again choose a horizontal line of length 2π in phase-space, follow the time evolution of each single phase-space point and record the number of kick-pulses for which the point stays bounded. For a given ensemble energy, E_0, this number is only a function of Θ and we denote it by $L(\Theta)$, the life time of the point (Θ, E_0). For $E_0 = -1/2$ and $\xi = 1$, the life time function L is displayed in Fig. 4. As mentioned in the introduction, this function is highly irregular and shows singularities on a fractal-like set of Θ-values. The fractal structure of L is demonstrated in Fig. 4b, which shows a blow up of the left-most feature in Fig. 4a.

An alternative way of showing visually the assignment of life times to phase-space points is to translate life times into a code of gray-values: the darker the shade of gray the longer the life time. The result of a scan over an area of $(\Theta, E)-$ phase-space can be seen in Fig. 5 and shows a fractal-like pattern which repeats itself on all scales. Our phase-space patterns are organized about the set Λ^+ of initial conditions for trajectories which never ionize. The closer an initial condition is to Λ^+, the longer it will remain bounded. The concept of two points being "close" to each other will be explained more precisely below. The darkest stripes in Fig 5. are the finite-N approximants of Λ^+. Similar patterns are known from the studies of chaotic scattering[6-9], and in order to make use of the existing concepts and techniques, we must extend our *ionization* problem in a way which will turn it (at least formally) into a *scattering* problem. This is done by endowing phase-space points (Θ_0, n_0) artificially with a past by means of T^{-1}, the inverse mapping of T. The extended problem admits forward as well as backward propagation and has a chaotic repeller, Λ, which is a "double fractal". The set Λ is called the invariant set since $T^N(\Lambda) \subset \Lambda$ for all $N \in \mathbf{Z}$. The set Λ^+ of our original problem is then nothing but the stable manifold of Λ and therefore has fractal features only along the unstable direction of *never-ionizing points*.

An element of Λ has to be necessarily a preimage- as well as an image-point of the mapping T. If we denote by I^{+1} the domain of the inverse mapping T^{-1}, the intersection of the domains of T and T^{-1}, $I = I^{-1} \cap I^{+1}$, is a superset for Λ. It is trivial to show that $I^{+1} = T(I^{-1})$. The set I^{+1} is shown in Fig. 1b as the shaded region of phase-space which appears as a system of infinitely many stripes. This is due to the action of the twist-mapping (2.18) and the fact, that the Kepler-frequency $1/n^3$ is singular for $n \to 0$. The set $I = I^{-1} \cap I^{+1}$, the union of the shaded stripes in Fig. 1c, contains all orbits of infinite length.

Due to the action of the twist-mapping, the set I is naturally partitioned into an infinite number of disjoint subsets which are labelled by $k = 1, 2, ...\infty$ (see Fig. 1c). To each point of the invariant set Λ we can assign a time-ordered sequence of the subsets k into which the point is mapped under the effect of $T^N, N = 1, 2, 3, ...$ and $T^{-N}, N = 1, 2, 3, ...$ Such a sequence contains in the zeroth position the k-label where the point can be found at the time $N = 0$, and tells its past and future in the course of the dynamical propagation. This description corresponds to a symbolic dynamics with an infinite alphabet. One can show that a trajectory may visit any k subset without restrictions imposed by its past history[44]. In other words, the formation of symbolic sequences which are relevant to our dynamics is not subjected to any grammatical restrictions.

As a consequence, each symbolic sequence which extends infinitely both to the left and to the right, represents at least one phase-space point $q \in \Lambda$. Each symbol sequence $...kkk...$ represents a fixed point of period one, each sequence $...k_1k_2k_1k_2...$ a fixed point of period two etc. Thus, the number of periodic orbits increases exponentially with the period length. Together with the hyperbolicity of T (see section 2) this proves that T belongs to the realm of systems with fully developed chaos[47].

We conjecture that the correspondence of infinite orbits and sequences is one-to-one, i.e., any arbitrarily selected sequence uniquely determines an orbit within Λ. Note that this statement is consistent with the hyperbolicity of T since it excludes the existence of elliptic periodic orbits. The orbital points of any hypothetical elliptic periodic orbit would be surrounded by islands of stability consisting of points with the same symbolic sequence in contradiction with the assumed one-to-one correspondence of phase-space points and symbolic sequences.

Returning to our ionization problem, which requires only forward mappings of phase-space points, we focus on the set Λ^+, the stable manifold of Λ. The iterates of some

starting point $p \in \Lambda^+$ are confined to I for all times $N \geq 1$, hopping from one k-subset of Λ to the next. This way, a grammatically unrestricted sequence of k-labels, extending from 1 to ∞ can be assigned to the forward orbit of p. Note that p itself is not necessarily an element of I^{+1} and therefore cannot in general be assigned a symbolic digit at the zeroth position of the sequence. The specification of the orbit of p for all times N' with $N' \leq N$ is done in terms of a symbolic string of length N and determines a stripe in phase-space in which p has to lie (compare Fig. 5). In order for the above asserted one-to-one correspondence of infinite sequences and points in Λ to hold, all the stripes have to be uniformly contracted as the length of the specified symbolic string is increased, such that for $N \to \infty$ one arrives at a one-dimensional set. We will provide strong evidence for the uniform contraction property at the end of this section.

We are now in a position to specify more precisely what is meant by an initial condition (Θ_0, n_0) being "close" to some point of Λ^+ : Two points (Θ_0, n_0) and (Θ_1, n_1) are said to be "close" to each other if they visit the same subsets k during the next K propagation steps, i.e., if the first K digits of their corresponding symbolic sequences are identical. The degree of closeness is measured by the magnitude of K.

In order to apply this criterion to arbitrary phase-space points, a slight extension of the symbolic dynamics is required: For any point $q \notin \Lambda^+$, the future orbit in the bounded space is finite. That point of its orbit, which is followed by the jump into the continuum, is an element of I^{+1}, but no more of I^{-1}, and hence not contained in any of the k-sets. Since we do not want to loose the dynamical information attached to this last orbital point, we will relate the *last digit* of any finite symbolic sequence to the partition of I^{+1} (shaded area in Fig. 1b) instead of I^{-1} (shaded area in Fig. 1c). The disjoint sub-sets of I^{+1} which extend from $\Theta = 0$ to $\Theta = 2\pi$, receive the label $\tilde{k}$ (see Fig. 1b). Since each set of the I^{+1}-partition contains exactly one k-set of the I^{-1}-partition as a subset, $\tilde{k}$ is chosen such as to fulfill $\tilde{k} \equiv k$ (see Figs. 1b,c).

Let us now use this symbolic dynamics for an understanding of the fractal stripe-pattern in Fig. 5. All areas of the same shade of gray consist of points with symbolic sequences of the same length. The darkest area ("black") in Fig. 5 represents the set of all points which did not ionize after the $N = 5$'th kick. Fig. 5, therefore, does not provide any stability information beyond the $N = 5$'th kick-pulse. In order to reveal the fractal structure hidden in the black area, we have to specify the behavior of its points for one more kick-pulse, i.e., we have to specify the $(N+1)$'th digit on top of the string of N digits

of the symbolic sequence. Because of the infinite alphabet of symbols and the absence of grammatical restrictions concerning the formation of sequences, we arrive at a partition of the stripe into infinitely many substripes, one of which consisting of initial points being ionized by the $(N+1)$'th kick-pulse. The $(N+2)$'th step will then remove a substripe of each of the substripes of the $(N+1)$'th generation, and so on.

In the following we investigate the life time function L on a horizontal line in phase-space which is characterized by E_0. It will be denoted by M_{E_0}. Since points in $M_{E_0} \cap \Lambda^+$ never ionize, the life time function will be singular on this set. Since Λ^+ consists of a bundle of curves (Θ, n) which extend over the whole range $0 < n < \infty$ and have a slope $dn/d\Theta > 0$ (see Fig. 5a for finite time approximants of Λ^+), the life time function of any selected horizontal line M_E represents by means of the set of its singularities the whole fractal structure contained in Λ^+. Let us denote by C_{E_0} the set given by such a horizontal cut through Λ^+ at the energy E_0. Following the iterative process which leads to C_{E_0} will answer the question: Which set of points on the line corresponds to a certain finite life time? Moreover, on the level of a one-dimensional cut through the fractal of Fig. 5, we are able to answer the following question: Given a symbolic sequence $k_1 \dots k_N$ of length N, what can be said about the position of $k_1 \dots k_N$ relative to the other stripes, and how can we determine the width of such a stripe?

We start with the set M_{E_0}. The first iteration step depletes the interval $M_{E_0} \setminus I^{-1}$ which consists of points which are transported into the continuum by the first kick. For the remaining set $M_{E_0} \cap I^{-1}$, the dynamical evolution over one kick-period is given by the mapping T. According to the results presented in section 2, $T(M_{E_0} \cap I^{-1})$ is composed of curves which extend from $\Theta = 0$ to $\Theta = 2\pi$ and have a small, monotonically negative slope. This is illustrated by the MCE (consisting of 200 equi-spaced points) shown in Fig. 1a whose image (full dots) is shown in Fig. 1b. With the help of the phase-space partitions which served as the basis for the symbolic dynamics, one easily verifies that each of these curves is a subset of one of the $\tilde{k}$-sets of the (I^{+1})-partition (see Fig. 1b), and that this correspondence is one-to-one. Therefore, according to our symbolic dynamics, all pre-image points of such a $\tilde{k}$-curve have the digit $\tilde{k}$ at the first position of their symbolic sequence. Recalling the continuity of the mapping T – which is veiled by the "modulo 2π"-prescription inherent in T_{twist} – we arrive at the coarsest level of structure imprinted on a horizontal line in phase-space by specifying the first symbol $\tilde{k}_1$ of the symbolic sequence: The left part of the interval M_{E_0}, $M_{E_0} \setminus I^{-1}$, consists of points for which the symbol

sequence is of length zero. The remainder, $M_{E_0} \cap I^{-1}$, is partitioned into an ordered set of infinitely many $\bar{k}_1$-intervals starting with $\bar{k}_1 = 1$.

For a more quantitative characterization of this partition, one has to know for any value of $\bar{k}_1$ the fraction of the image-set $T(M_{E_0} \cap I^{-1})$ which is represented by the $\bar{k}_1$-curve. This fraction can be calculated approximately in two steps:

i) Projecting the two-dimensional $\bar{k}$-sets onto the energy-axis and treating the overlap in a consistent way, the $\bar{k}$-partition of I^{+1} can be translated into a $\bar{k}$-partition of the energy-axis.

ii) Formula (3.1) tells us, how the points of $T(M_{E_0} \cap I^{-1})$ are distributed over the energy E' and therefore, how $T(M_{E_0} \cap I^{-1})$ is distributed among the $\bar{k}$-intervals on the energy axis which were obtained in step i).

Within the framework of the Markovian approximation of section 3, the whole process is iterative. According to section 3, each $\bar{k}$-subset of $T(M_{E_0} \cap I^{-1})$ can be well aproximated by a MCE. This assigns to each symbol $\bar{k} \in \mathbf{N}$ a MCE M_{E_k} according to the $\bar{k}$-partition of the energy-axis (cf. i) above). Since this way the initial condition for the next iteration of T is identical with the starting condition, the specification of one more symbolic digit for the points on the initial horizontal line is equivalent with another application of the above described procedure.

The essence of this procedure can be summarized as follows: Let an ensemble of trajectories be characterized by the symbol sequence $k_1 \ldots k_{N-1}\, \bar{k}_N$. Then, the partition of this ensemble under the $(N+1)$'th application of the mapping T depends only on the $\bar{k}_N$ image set in which all the orbits of the ensemble reside prior to the $(N+1)$'th application of the mapping T. Thus, the behavior of the ensemble under the $(N+1)$'th application of T is completely determined by the last symbol $\bar{k}_N$ in the sequence. This means that the pre-history, i.e., the symbols $k_1, \ldots, k_{N-1}$ are not important for the future time evolution. This, of course, is nothing but a statement on the approximately Markovian nature of the dynamics on the level of symbolic strings. Therefore, the partition scheme can be represented in the form of a $\infty \times \infty$-matrix A which does not depend on the iteration step N. Each symbol $\bar{k}_N \in \mathbf{N}$ is represented by a raw in A which reflects the branching ratios of the MCE $M_{E_{k_N}}$ into the different "channels" such as decay into the continuum or redistribution into the different $\bar{k}_{N+1}$-sets with $\bar{k}_{N+1} \in \mathbf{N}$. Therefore, and to a good approximation, subsequent applications of T form a Markov chain with the transition matrix A.

If the initial horizontal cut in (θ, E)-phase space is chosen to be identical with one of the $M_{E_{k_0}}$ ensembles, the length of an arbitrary subinterval consisting of points characterized by the symbol sequence $k_1 \dots k_{N+1} \bar{k}_N$, can be determined directly on the basis of the transition matrix A: The length of the interval is simply 2π times the product of the N transition matrix elements $(\bar{k}_0 \to \bar{k}_1)(\bar{k}_1 \to \bar{k}_2) \dots (\bar{k}_{N-1} \to \bar{k}_N)$.

Concluding this section, we present some arguments in support of the conjecture that any infinitely extended symbol sequence $k_1 \dots k_\infty$ corresponds to a one-dimensional curve in (θ, E)-phase space. In other words, we have to disprove the existence of hypothetical two-dimensional regions in this set of points. We distinguish two cases:

a) The symbol sequences $k_1 \dots k_\infty$ are constructed from a finite alphabet of symbols.

b) The alphabet is infinite.

For case a) let us again consider a horizontal cut through the set $k_1 \dots k_\infty$. The length of this interval is estimated with the help of the transition matrix A. According to the limited set of symbols in this case, the number of transition matrix elements involved is finite, too. Denote the largest of these matrix elements by λ. Since all transition matrix elements are smaller than 1, we have $\lambda < 1$. The length of an interval which corresponds to a sub-sequence $k_1 \dots k_N$ in $k_1 \dots k_\infty$ is therefore bounded by $2\pi\lambda^N$. For $N \to \infty$, this estimate approaches zero. This shows that within the Markovian approximation the horizontal extent of the set $k_1 \dots k_\infty$ is zero everywhere and $k_1 \dots k_\infty$ is thus a one-dimensional curve.

In case b) the sequence $k_1 \dots k_\infty$ contains symbols which surpass any natural number. On the other hand, using area conservation of the mapping T in (θ, E)-phase space, we have: Area of the pre-image set $k_1 \dots k_\infty$ < area of the pre-image stripe $k_1 \dots k_N$ = area of the image set $T^N(k_1 \dots k_N)$ < area of the $\bar{k}_N$-image set of the I^{+1}-partition. Close inspection of the partition of the set I^{+1} shows that for $\bar{k}_N \to \infty$ the area of the $\bar{k}_N$-sets approach zero. Therefore, even in case b), $k_1 \dots k_\infty$ is a one-dimensional curve.

5. The Anomalous Scaling of the Hydrogen Fractal

In the previous two sections we presented two seemingly unrelated aspects of the ionization process of the classically described kicked Hydrogen atom. In section 3 we studied the decay of phase space ensembles. We found that classical MCE's decay algebraically in time. In section 4 we investigated the fractal set Λ^+ of points which remain bound for ever. In the present section we will show that there is an intimate connection between these two subjects. We will show that because of the powerlaw decay obtained in section 3, the set

A^+ is a fractal with rather uncommon properties. As a matter of fact, since scaling fractals lead to exponential decay, the hydrogen fractal (see Fig. 5) cannot be a scale-invariant fractal. Hence, it must belong to the class of fractal-like sets with broken scaling-symmetry. Only the broken scaling symmetry allows for an algebraic decay of the Lebesgue-measure in the course of the fractal-generating process. We note that although the fractal displayed in Fig. 5 consists of many subintervals in every step of its generation, it cannot be a multi-scale fractal[3] since there are no fixed scaling relations. Also, a multi-scale fractal would again lead to exponential decay.

The mathematical description of fractals with broken scaling symmetry requires the introduction of concepts which are not commonly used in the physics literature. We shall briefly review these concepts below, and refer the interested reader to Ref. 23 for further details.

Self-similar fractals can be adequately characterized by their Hausdorff-dimension d_0, which is closely related to the d-dimensional measure of a fractal set C. Let C be embedded in a D-dimensional space and consider coverings of C by D-dimensional boxes of length ϵ. For an arbitrary positive and real number d, the d-dimensional measure of C is defined as

$$\mu^{(d)} = \lim_{\epsilon \to 0} N(\epsilon)\, \epsilon^d \quad , \tag{5.1}$$

where $N(\epsilon)$ is the smallest number of ϵ-boxes that is sufficient to cover C. There exists a critical value of d, say d_0, such that $\mu^{(d)}$ is infinite for all $d < d_0$ and zero for all $d > d_0$. This critical exponent d_0 is called the Hausdorff-dimension of C. The definition given above does not ensure that the d_0-dimensional Hausdorff measure $\mu^{(d_0)}$ is finite. Sets with broken scaling symmetry require a generalization of definition (5.1) in order to achieve finiteness of the Hausdorff measure. In order to counterbalance the proliferation of ϵ-boxes when performing the limit $\epsilon \to 0$, the class of functions ϵ^d has to be extended to a wider class of functions $\lambda(\epsilon)$, resulting in the Hausdorff measure with respect to a gauge function λ :

$$\mu_\lambda = \lim_{\epsilon \to 0} N(\epsilon)\, \lambda(\epsilon) \tag{5.2}$$

The particular function λ which yields a finite μ_λ is called the intrinsic gauge function of the set C. For a large class of anomalously scaling fractals the intrinsic gauge functions are contained in the following expansion scheme:

$$\lambda(\epsilon) = \epsilon^{d_0} \cdot \prod_{k=1}^{n} \left[\ln^k\left(\frac{1}{\epsilon}\right)\right]^{-d_k} = \exp\left(\ln(\epsilon) d_0 - \ln(\ln\left(\frac{1}{\epsilon}\right)) d_1 - \ldots\right) \tag{5.3}$$

Thus, a large class of sets with broken scaling symmetry can be characterized in terms of exponents $d_0, d_1, ...$, where $d_1, d_2, ...$ are the coefficients of higher order logarithmic corrections to the usual Hausdorff-dimension d_0.

A canonical way[23] to generate an anomalously scaling fractal C is based on the iterative middle third mechanism given by Cantor. In Cantor's original example[14-16], the iteration steps consist of taking out a constant fraction, say one third, from the middle of each interval. By allowing the deleted fraction to display a dependence on the number N of the iteration step, the dependence being described in terms of the so-called hole function h_N, the resulting fractal (in general) is no more scaling, and a logarithmic correction to the power law in the set's gauge function arises. For example, the hole function $h_N = \frac{c}{N}$, where $c \in (0,1)$ is a constant, generates a fractal object characterized by the exponents $d_0 = 1$, $d_1 = -c$, and $d_l = 0$ for all $l > 1$. This means, that the algebraic decay of the Lebesgue-measure during the fractal-generating process is too slow to alter the dimension $d_0 = 1$ of the interval one starts with, but that this algebraic decay nevertheless gives rise to zero linear extent (i.e. zero Lebesgue-measure) of the resulting fractal. The "fractal" nature of the resulting set is given quantitatively by the first logarithmic correction d_1.

In order to get a grip on the fractal properties of a given set, the concept of the uncertainty dimension defined in Ref. 12 turns out to be particularly useful. Based on this technique we will present below numerical evidence for the conjecture that the hydrogen fractal displayed in Fig. 5 has a broken scaling symmetry.

The procedure for calculating the uncertainty dimension of a fractal set C embedded in a one-dimensional covering space U (a straight line segment whose length is assumed to be normalized to 1) is as follows[12]: Choose a set of points $p_j \in U, j = 1, ..., Q$ equidistributed in U. A point $p \in U$ is ϵ-certain, if p and the two neighboring points $p_- = p - \epsilon$ and $p_+ = p + \epsilon$ have the same life time in U. The point p is called ϵ-uncertain, if any two of p, p_- or p_+ differ in their respective life times. With the help of the function

$$\psi_\epsilon(p) = \begin{cases} 0, & \text{if } p \text{ is } \epsilon\text{-certain} \\ 1, & \text{if } p \text{ is } \epsilon\text{-uncertain} \end{cases} \tag{5.4}$$

we define the function

$$f(\epsilon) = \frac{1}{Q} \sum_{j=1}^{Q} \psi_\epsilon(p_j) \quad , \tag{5.5}$$

which is the ratio of the number of ϵ-uncertain points to the total number of points. (Note that the usual definition of ϵ-certainty requires that the function at p_+ differs from its

value at p_- by less than a fixed amount δ. In our case the function L assumes only integer values, and therefore one can require strict equality).

The function $f(\epsilon)$ is intimately connected with the question of how many intervals of length ϵ are necessary to cover C. The following heuristic arguments explain the connection. C is the set of all points in U whose life time is infinite. In order to cover C, all points of equal ($\equiv$ finite) life time can thus be subtracted from the line segment U as far as a covering of C is concerned. The total length of these intervals is nothing but the fraction of ϵ-certain points, i.e., $1 - f(\epsilon)$. This argument shows immediately that $f(\epsilon)$ is the ratio of $N(\epsilon)$, the number of ϵ-intervals necessary for covering C, and $1/\epsilon$, the number of ϵ-intervals in U. In the limit $\epsilon \to 0$ we have

$$f(\epsilon) \sim N(\epsilon)/(1/\epsilon) = \epsilon\, N(\epsilon) \quad . \tag{5.6}$$

Since for a scaling fractal $N(\epsilon) \sim \epsilon^{-d_0}$ (see (5.1)) we obtain[12]

$$f(\epsilon) \;\sim\; \epsilon^{\gamma} \quad , \tag{5.7}$$

where $\gamma = 1 - d_0$ is the uncertainty dimension of the fractal set.

Applying the concept of the uncertainty dimension to our ionization problem, we calculated $f(\epsilon)$ for $C = C_{n_0} = E_{n_0} \cap \Lambda^+$. We chose $n_0 = 1.1$ and $\xi = 1$. Fig. 6a shows $\ln(f(\epsilon))$ vs. $\ln(\epsilon)$ over several decades in ϵ. If C_{n_0} were a scaling fractal, the data points shown in Fig. 6a should lie on a straight line. Clearly this is not the case. Fig. 6b shows $\ln(f(\epsilon))$ plotted against $\ln(\ln(1/\epsilon))$. This time we obtain asymptotically a straight line which proves that

$$f(\epsilon) \sim e^{-\mu \ln(\ln(1/\epsilon))} \;=\; [\ln(1/\epsilon)]^{-\mu} \tag{5.8}$$

with $\mu \approx 1.2$. Comparing (5.8) with the expansion (5.3) of the gauge function $\lambda_0(\epsilon) \sim N(\epsilon)^{-1} \sim \epsilon\, f(\epsilon)^{-1}$, the Hausdorff-dimension of C_{n_0} is seen to be given by $d_0 = 1$, and $-\mu$ is nothing but the first logarithmic correction term d_1. Since C_{n_0} is only a one-dimensional cut through the hydrogen fractal displayed in Fig. 5, the numerical value of d_1 (≈ -1.2 for $n_0 = 1.1$) can still depend on n_0. On the other hand we expect that the global properties of the fractals C_{n_0} are structurally stable with respect to the precise location n_0 of the cut. Thus, the kicked hydrogen atom is an example for the appearance of a fractal with broken scaling symmetry in a physical nonlinear system.

Despite the close analogy between the modified Cantor set described in Ref. 23 and the invariant set Λ^+ of the kicked H-atom, there is a fundamental difference. In the schematic

model of Ref. 23, the algebraic decay of the Lebesgue-measure hinges on an explicitly time dependent *hole function* h_N; the algebraic decay was "put in by hand". For the positively kicked H-atom, however, it was shown in section 4 that the fractal generating mechanism can be written in the form of a transition matrix which is *not* dependent on N. The question arisis, how in this case an algebraic decay is possible at all?

Consider the ensemble of points whose life time is longer than N and therefore possesses a symbolic sequence $k_1 \ldots k_N$. For increasing N, the weight within such an ensemble will shift to symbolic sequences with higher and higher values of k_N. This effect is purely dynamical. On the level of the random walk model, it corresponds to a drift to lower and lower energies (see section 3). But since the transition probabilities to the continuum decrease with increasing k_N, an algebraic decay results.

We conclude that a fractal generating mechanism, defined by a time independent symbolic dynamics, can lead to powerlaw decay only if its alphabet is infinite. Only in this case, a shift of phase-space probability to ever higher symbols is possible and provides the basis for algebraic decay in a purely hyperbolic system.

6. Driving with pulses of finite width

During the last two decades of intensive activity in studying the response of Rydberg atoms to periodic driving fields, the experimental work concentrated on *mono-chromatic* driving[38,48–52] with a few exceptions where bi-chromatic driving was also studied[53]. It took quite a long time till reliable theoretical and computational tools were developed to match and interpret the experimental findings. In the interim period a few groups studied the kicked H-atom *model*[39,40,42–44,54] in an attempt to emulate some of the features observed experimentally. It was soon found out, however, that the two problems are markedly different, and due to the Coulomb singularity, the kicked H-atom cannot be considered as an approximate description of the mono-chromatically driven atom in any reasonable way[55].

The kicked H-atom is an interesting system in its own right, displaying surprising features, some of which were illustrated in the preceeding sections. The realization of narrow pulses in laboratory experiments seems to be feasible now, and it is interesting to find out which features of the idealized δ-kicks model are robust against the replacement of the δ-kicks by smooth pulses. In the sequel we shall show that the power-law decay is such a quantity: it can be observed over a long time interval, even when the H-atom is driven by a train of smooth impulses.

In order to demonstrate the feasibility of the proposed impulsive driving experiments, we replaced the periodic δ-kicks in (2.8) by smooth periodic Gaussian pulses of width σ:

$$\delta_{2\pi}(\tau/\xi) \;\rightarrow\; g_{2\pi}^{(\sigma)}(\tau/\xi) \;=\; \frac{1}{\sqrt{2\pi}\sigma}\, e^{-\tau^2/2\sigma^2\xi^2}; \qquad -\pi \leq \tau/\xi \leq \pi \quad . \tag{6.1}$$

Accordingly, the kick-mapping T defined in (2.17) is replaced by a mapping $T^{(\sigma)}$. Of primary importance for the proposed experiments is to know the order of magnitude of the pulse width σ which is necessary for observing the powerlaw decay originating from the hyperbolic mechanism discussed in the previous sections. To answer this question, we ran several Monte Carlo simulations with $\xi = 1$ and $E_0 = -1/2$. For two cases, $\sigma = 0.04$ and $\sigma = 0.002$, the resulting decay curves are shown in Figs. 7a and 7b, respectively. The decay curves (full lines) can be compared directly with the decay curves for δ-kicks (dashed lines). Both finite width decay curves show an initial offset from the decay curves corresponding to the kicked (zero-width) case since finite-width pulses are not as effective for ionization as δ-kicks. The finite-width decay curves subsequently run parallel to the kick-curve, apparently emulating the hyperbolic decay mechanism. Note, that the $\sigma = 0.002$-curve runs closer to the kick-curve (and for a longer time) than the $\sigma = 0.04$-curve since due to its smaller width it ionizes more effectively than the $\sigma = 0.04$ pulses. The slopes of both decay curves in this initial phase are very close to the value $\alpha = 1.65$ characteristic for the zero-width case. After this initial phase, the decay in both cases accelerates and the corresponding decay curves bend toward an algebraic decay with an asymptotic decay power of $\alpha \approx 2.1$. The critical time at which the bending occurs will be denoted by $N_c^{(\sigma)}$. Fig. 7 shows that $N_c^{(\sigma=0.04)} < N_c^{(\sigma=0.002)}$, i.e., the narrower width pulses follow the prediction of the kick-model over a considerably longer time. The reason for the deviation from the predictions of the kick-model becomes apparent if we monitor the average action of an ensemble of classical trajectories as a function of time. Fig. 8 shows the ensemble average of the action, $< n >$, for the case $\sigma = 0.04$. It is seen that the action is bounded from below, which is due to the fact that $T^{(\sigma)}$ is not hyperbolic. The non-hyperbolicity of $T^{(\sigma)}$ is easily demonstrated with the help of a phase-space portrait of $T^{(\sigma)}$ which, for $\sigma = 0.04$, is shown in Fig. 9. Apparently, the phase-space of $T^{(\sigma)}$ possesses regular and chaotic regions. Actions below a critical action $n_c^{(\sigma)}$ are not accessible due to the existence of sealing KAM surfaces (see Fig. 9). This explains the saturation of $< n >$ at $< n > \approx n_c^{(\sigma=0.04)} \approx 0.41$.

The critical action $n_c^{(\sigma)}$ at which the shielding KAM curves become active can easily be estimated by expanding the form factor of the driving pulses, $g_{2\pi}^{(\sigma)}(\tau/\xi)$, into a Fourier

series according to

$$g_{2\pi}^{(\sigma)}(x) \;=\; \frac{1}{2}b_0 \;+\; \sum_{m=1}^{\infty} b_m \cos(mx) \quad . \tag{6.2}$$

For narrow width pulses, the Fourier amplitudes b_m are approximately given by

$$b_m \;\approx\; \frac{1}{\pi}\int_{-\infty}^{\infty} g^{(\sigma)}(x)\cos(mx)\,dx \;=$$

$$\frac{1}{\pi}\int_{-\infty}^{\infty}\frac{1}{\sqrt{2\pi}\sigma}\,e^{-x^2/2\sigma^2}\cos(mx)\,dx \;=\; \frac{1}{\pi}\,e^{-(m\sigma)^2/2} \quad . \tag{6.3}$$

This result shows that the amplitudes b_m vanish quickly for $m > m_c^{(\sigma)} \sim 1/\sigma$. The angular frequency of the fundamental harmonic in (6.1) is $\Omega = 1/\xi$. The $m_c^{(\sigma)}$'th harmonic excites a primary resonance of the one-dimensional hydrogen atom at $[1/n_c^{(\sigma)}]^3 = m_c^{(\sigma)}/\xi$, which implies $n_c^{(\sigma)} \sim (\sigma\xi)^{1/3}$. For $n < n_c^{(\sigma)}$, the $m_c^{(\sigma)}$'th harmonic acts as an adiabatic perturbation which implies the existence of shielding KAM curves in this action region.

In order to check the $\sigma^{1/3}$-scaling of $n_c^{(\sigma)}$, we plotted five additional phase-space portraits analogous to Fig. 9 to obtain numerically the onset of the KAM-curves for all together six different pulse widths: $\sigma = 0.15, 0.10, 0.04, 0.02, 0.01$, and 0.002. We obtained $n_c^{(\sigma)} = 0.65, 0.56, 0.41, 0.33, 0.26$, and 0.15, respectively. For the six ratios $n_c^{(\sigma)}/\sigma^{1/3}$ we obtain 1.22, 1.21, 1.20, 1.22, 1.21, 1.19, respectively, which confirms the $\sigma^{1/3}$-scaling to a very good accuracy.

The shielding of n-values with $n < n_c^{(\sigma)}$ explains in a natural way the existence of a critical time $N_c^{(\sigma)}$ from which on ($N > N_c^{(\sigma)}$) an acceleration of the decay is observed (see Fig. 7). As soon as the tail of the energy distribution function $f^{(\sigma)}(E,N)$ (the distribution function $f(E,N)$ for finite width σ) has reached the blocking KAM curves at $n \approx n_c^{(\sigma)}$, which happens at $N \approx N_c^{(\sigma)}$, the mechanism presented in this paper and based on the hyperbolicity of T has to compete with the mechanism discussed in Refs. 25-29 which applies to a mixed phase-space. The latter mechanism is clearly the relevant mechanism once the probability has drifted toward the "sticky" boundary layer at $n \approx n_c^{(\sigma)}$.

The critical times $N_c^{(\sigma)}$ which mark the cross-over between the two powerlaw regimes can be extracted easily if the data presented in Fig. 7 are rescaled by compensating the initial decay of the finite-σ decay curves which emulates the hyperbolic δ-kick mechanism. We define the *compensated decay function*:

$$R^{(\sigma)}(N) \;=\; r^{(\sigma)}\,N^{s^{(\sigma)}}\,P_B^{(\sigma)}(N) \quad . \tag{6.4}$$

The normalization constant $r^{(\sigma)}$ is not important and can be chosen arbitrarily for a convenient presentation of the compensated decay function (see Fig. 10). The exponent $s^{(\sigma)}$, which is expected to be close to 1.65 (the value compensating the decay due to kicks), compensates the initial decay of $P_B^{(\sigma)}(N)$ which (for small σ) is mainly due to the hyperbolic mechanism. The resulting *compensated decay curves* for three choices of σ are displayed in Fig. 10. The existence of a transition in $P_B^{(\sigma)}(N)$ between two powerlaw regimes is apparent. After an initial plateau corresponding to the prevailance of the hyperbolic mechanism all three curves bend up sharply at their respective $N_c^{(\sigma)}$ reaching an asymptotic slope close to $\alpha = 2.1$. For $\sigma = 0.04$, the transition occurs at $N_c^{(\sigma=0.04)} \approx 6$. For $\sigma = 0.01$ and $\sigma = 0.002$ we obtain $N_c^{(\sigma=0.01)} = 12$ and $N_c^{(\sigma=0.002)} = 25$, respectively. The sharp bend and the ensuing linear behavior in $\ln(R^{(\sigma)})$ vs. $\ln N$ for $N > N_c^{(\sigma)}$ indicates the transition to the Cantorus diffusion mechanism[25-29] which is based on the picture of slow diffusion of phase-space probability in and out of a hierarchy of Cantori and island chains. In Ref. 44 this evidence is corroborated by a sequence of time resolved phase space portraits which show explicitly the sticking of trajectories to the regular structures at $n \approx n_c$ for times $N > N_c^{(\sigma)}$. The observed exponent $\alpha \approx 2.1$ (see Fig. 10) in the finite-width case is consistent with the results presented in Refs. 25-29.

The scaling of the critical times $N_c^{(\sigma)}$ with σ can be obtained in the following way. It is easy to show that the Fokker-Planck equation (3.4) possesses solutions $f(E,N)$ which scale in E/N. One such solution, e.g., would be $f(E,N) \sim \gamma(-5/2, \xi E/N)$, where γ is the incomplete gamma-function. These solutions do not, in general, fulfill the boundary conditions (3.5). Also, they apply strictly only for the case of δ-kicks. These draw-backs, however, are probably of little concern for the scaling of the tails of the distribution function $f^{(\sigma)}(E,N)$ as long as $N < N_c^{(\sigma)}$ and therefore $|E| < |E_c^{(\sigma)}| = 1/2(n_c^{(\sigma)})^2$. Assuming E/N-scaling, the variance of $f(E/N)$ scales like N^3 and the energy spread of f scales like $N^{3/2}$. Therefore, the magnitude of the probability function f becomes appreciable at the critical energy $E_c^{(\sigma)}$ after times $N_c^{(\sigma)} \sim |E_c^{(\sigma)}|^{2/3} \sim 1/(n_c^{(\sigma)})^{4/3}$. This implies the scaling relation $N_c^{(\sigma)}\sigma^{4/9} = const.$ As mentioned above, Fig. 10 shows that $N_c^{(\sigma)} = 6, 12, 25$ for $\sigma = 0.04, 0.01, 0.002$, respectively. For the scaling product we obtain: $N_c^{(\sigma)}\sigma^{4/9} = 1.4, 1.6, 1.6$, respectively, which confirms the above considerations to a good accuracy.

7. Summary and conclusions

The main result of this paper is that the survival probability of a set of phase-space points decays like a powerlaw under the influence of a hyperbolic mapping T. As a conse-

quence, a widely accepted working hypothesis which assigns exponential decay to hyperbolic systems[13,20,21,24] and algebraic decay to regular systems[13] has to be revised. The symbolic description of the dynamics of our system requires an alphabet with an infinite number of symbols. This explains the observed powerlaw decay. The hyperbolicity of T was proved analytically. To our knowledge this is the first time that the hyperbolicity of a physically relevant system was demonstrated exactly. Moreover, we were able to construct an analytically solvable Markovian model which closely approximates the dynamics of T. Solving analytically a first passage time equation, the exponent of the algebraic decay was predicted to be 3/2. This agrees very well with the numerical data which point to an exponent in the vicinity of 1.65. The algebraic decay was then interpreted within the framework of fractal theory. The invariant set of T was identified as a fractal set with broken scaling symmetry. The first logarithmic correction to the fractal dimension of the invariant set was determined numerically with the help of the method of the uncertainty dimension. Finally, we extended our investigations to the case of periodic pulses of finite width. The existence of a cross-over between two powerlaw regimes was established.

We hope that apart from clarifying a theoretical issue concerning the decay properties of classical sets in chaotic systems, our results can be tested experimentally. An ionization experiment with Rydberg atoms perturbed by a train of finite-width microwave pulses appears to be a promising candidate.

Acknowledgements

We gratefully acknowledge helpful discussions with T. Tél, C. Grebogi, M. Bellermann, L. Moorman, P. M. Koch and A. Schenzle. C. F. H. and U. S. acknowledge financial support by Stiftung Volkswagenwerk. R. B. is grateful for financial support by the Deutsche Forschungsgemeinschaft and by the NSF under grant number CHE88-19436.

Figure Captions

Fig. 1: a) The domain I^{-1} of the mapping T (shaded area) and a microcanonical straight-line ensemble $M_{E_0} \cap I^{-1}$. b) The image $I^{+1} = T(I^{-1})$ of the domain of T and the image $T(M_{E_0} \cap I^{-1})$. The $\tilde{k}$-labels of the stripe structure are shown on the right hand side of the frame. c) The set $I = I^{+1} \cap I^{-1}$ and the k-labels of the stripe-structure. The stripe pattern continues for $E < -1.5$ such that $k, \tilde{k} \to \infty$ for $E \to -\infty$.

Fig. 2: Survival probability $P_B(N)$ vs. the number of kicks N for five different initial straight-line ensembles $n_0 = 1.0, 0.5, 0.25, 0.1$ and 0.05, respectively. The ensembles consist of $3 \cdot 10^5$ points each and $\xi = 1$.

Fig. 3: Test of the stochastic model and its predictions for the scaling of the decay curves of periodically kicked hydrogen atoms. Full line: Survival probability G as a function of scaled time z as predicted by the stochastic model. The five plot symbols $+ \diamond \triangle \sqcap \bigcirc$ correspond to the five initial straight-line ensembles $n_0 = 1, 0.5, 0.25, 0.1$ and $n_0 = 0.05$, respectively, whose decay curves are displayed in Fig. 2. The plot-sympols represent survival probabilities at selected values of N taken from Fig. 2. Data was taken for $n_0 = 1$ at $N = 1, 5, 20, 70, 200$, for $n_0 = 0.5$ at $N = 1, 10, 50, 100, 200, 500$, for $n_0 = 0.25$ and $n_0 = 0.1$ at $N = 1, 10, 50, 100, 500$ and for $n_0 = 0.05$ at $N = 1, 50, 200, 500$ and 1500.

Fig. 4: Life time function $L(\Theta)$ for $E = -1/2$ ($n_0 = 1$). $L(\Theta) = 0$ for $\Theta < \pi$. a) Full range $\pi \leq \Theta \leq 2\pi$. b) Blow up of the left-most feature in a). L shows structure on all scales.

Fig. 5: Two-dimensional visualization of $L(\Theta, E)$. The life times $L = 1, 2, ..., 5$ are visualized with the help of 5 shades of gray indicating the fractal properties of $L(\Theta, E)$. b) Blow up of a detail in frame a).

Fig. 6: The fraction, f, of ϵ-uncertain points vs. ϵ for the ensemble $M_{n_0} \cap I^{-1}$ with $n_0 = 1.1$ and $\xi = 1$. a) A log-log-plot of f vs. ϵ shows that the H-fractal is not a scaling fractal. b) A double-log scale in ϵ reveals that $\ln(f)$ scales in $\ln\ln(1/\epsilon)$.

Fig. 7: Decay curves for finite width pulses (full lines) in direct comparison with decay curves for δ-kick driving (dashed lines). a) $\sigma = 0.04$, b) $\sigma = 0.002$.

Fig. 8: The ensemble average $< n >$ of the action n as a function of the number of pulses N for finite width pulses with $\sigma = 0.04$. Occasional spikes are due to very highly excited trajectories which are on their way to ionization and dominate the average for a short while.

Fig. 9: Phase-space portrait of a one-dimensional H-atom driven by a finite width pulse of Gaussian shape with $\sigma = 0.04$ and $\xi = 1$. The phase-space contains regular and chaotic regions and shows sealing KAM curves for $n \lesssim 0.4$.

Fig. 10: Demonstration of the cross-over between the hyperbolic and the Cantorus powerlaw regimes for smooth pulse drive by means of three compensated decay curves $R^{(\sigma)}$ with a) $\sigma = 0.04, 0.01$ and b) $\sigma = 0.002$. In frame b) the compensated decay curve for kicks (dashed line) is also shown. The cross-over from the hyperbolic to the Cantorus mechanism occurs at $N_c^{(\sigma)} \approx 6, 12, 25$ for the three cases $\sigma = 0.04, 0.01$ and 0.002, respectively. The scaling factors $r^{(\sigma)}$ and $s^{(\sigma)}$ were chosen to be independent of sigma: $r^{(\sigma)} = r = 1.52$ and $s^{(\sigma)} = s = 1.55$. For the compensated kick-curve (dashed line in frame b), we chose r=1.52 and s=1.65.

References

1) B. B. Mandelbrot, Physica **D7**, 224 (1983).

2) H.-O. Peitgen and P. H. Richter, "The beauty of fractals" (Springer, Berlin/Heidelberg, 1986).

3) T. Tél, Z. Naturforsch. **43a**, 1154 (1988).

4) E. Lorentz, J. Atm. Sci. **20**, 130 (1963).

5) C. Sparrow, "The Lorenz Equations, Bifurcations, Chaos, and Strange Attractors (Springer, New York, 1983).

6) B. Eckhardt, Physica **D33**, 89 (1988).

7) U. Smilansky, in "Chaos and Quantum Physics", edited by A. Voros, M. Gianonni and O. Bohigas, NATO, Les Houches Lecture Notes (North-Holland, 1990).

8) R. Blümel, in "Directions in Chaos", Vol. 4, edited by B.-L. Hao, D. H. Feng and J.-M. Yuan, (World Scientific, Singapore, 1991).

9) T. Tél, in "Directions in Chaos: Experimental Study and Characterization of Chaos", Vol. 3, edited by Hao Bai-Lin, (World Scientific, Singapore, 1990) pp. 149.

10) Y. Gu and J.-M. Yuan, Phys. Rev. **A36**, 3788 (1987).

11) J. Heagy and J.-M. Yuan, Phys. Rev. **A41**, (1990).

12) S. W. McDonald, C. Grebogi, E. Ott and J. A. Yorke, Physica **D17**, 125 (1985).

13) W. Bauer and G. F. Bertsch, Phys. Rev. Lett. **65**, 2213 (1990).

14) G. Cantor, Mathematische Annalen **21**, 545 (1883).

15) G. Cantor, "Grundlagen einer allgemeinen Mannigfaltigkeitslehre. Ein mathematisch-philosophischer Versuch in der Lehre des Unendlichen." B. G. Teubner, Leipzig, 1883, in: "Gesammelte Abhandlungen mathematischen und philosophischen Inhalts", edited by E. Zermelo (Springer, Berlin, 1966) p. 207.

16) G. Cantor, "Über unendliche lineare Punktmannigfaltigkeiten", part 6, Mathematische Annalen **23**, 453 (1884), in Ref. 14a, p. 235.

17) B. B. Mandelbrot, "Fractals: Form, Chance, and Dimension", (Freeman, San Francisco, 1977).

18) A. J. Lichtenberg and M. A. Lieberman, "Regular and Stochastic Motion", Applied Math. Sci. **38** (Springer, New York, 1983).

19) J. Guckenheimer and P. Holmes, "Nonlinear Oscillations, Dynamical systems and Bifurcations of Vector Fields", Appl. Math. Sci. **42** (Springer, NY 1983).

20) T. Tél, J. Phys. **A22**, L691 (1989).

21) T. Tél, Phys. Rev. **A36**, 1502 (1987).

22) C. Hillermeier and R. Blümel, in "Fundamentals of Laser Interactions II", Lecture Notes in Physics, Vol. 339, p. 305, edited by F. Ehlotzky (Springer, New York, 1989).

23) D. K. Umberger, G. Mayer-Kress, and E. Jen, in "Dimensions and Entropies in Chaotic Systems", edited by G. Mayer-Kress, Springer Series in Synergetics (Springer, New York, 1986), p. 47, example 1.2.

24) Y.-T. Lau, J. M. Finn, and E. Ott, Phys. Rev. Lett. **66**, 978 (1991).

25) C. F. F. Karney, Physica **D8**, 360 (1983).

26) B. V. Chirikov and D. L. Shepelyansky, Physica **D13**, 395 (1984).

27) J. D. Meiss and E. Ott, Phys. Rev. Lett. **55**, 2741 (1985).

28) J. D. Meiss and E. Ott, Physica **D20**, 387 (1986).

29) J. D. Hanson, J. R. Cary, and J. D. Miess, J. Stat. Phys. **39**, 327 (1985).

30) D. L. Shepelyansky, in *Chaotic Behavior in Quantum Systems*, ed. by G. Casati, p. 187 (Plenum, New York, 1985).

31) R. V. Jensen, Phys. Rev. Lett. **49**, 1365 (1982).

32) R. V. Jensen, Phys. Rev. **A30**, 386 (1984).

33) G. Casati, B. V. Chirikov, D. L. Shepelyansky and I. Guarneri, Phys. Rep. **154**, 77 (1987).

34) R. Blümel and U. Smilansky, Z. Phys. **D6**, 83 (1987).

35) R. Blümel, C. Hillermeier and U. Smilansky, Z. Phys. **D15**, 267-280 (1990).

36) G. Casati, B. V. Chirikov, and D. L. Shepelyansky, Phys. Rev. Lett. **53**, 2525 (1984).

37) J. N. Bardsley and M. J. Comella, J. Phys. **B19**, L565 (1986).

38) J. N. Bardsley, B. Sundaram, L. A. Pinnaduwage, and J. E. Bayfield, Phys. Rev. Lett. **56**, 1007 (1986).

39) R. Blümel and U. Smilansky, Phys. Rev. Lett. **52**, 137 (1984).

40) R. Blümel and U. Smilansky, Phys. Rev. **A30**, 1040 (1984).

41) I. C. Percival and D. Richards, Adv. At. Mol. Phys. **11**, 1 (1975).

42) A. Carnegie, J. Phys. **B17**, 3435 (1984).

43) K. Zyczkowski and J. Zakrzewski, J. Phys. **A21**, L371 (1988).

44) C. F. Hillermeier, Ph. D. thesis, Ludwig-Maximilians-Universität, München, 1991.

45) C. W. Gardiner, Handbook of Stochastic Methods, 2nd edition, (Springer, Berlin, 1985).

46) I. S. Gradshteyn and I. M. Ryzhik, "Table of Integrals, Series, and Products" (Academic Press, New York, 1980).

47) S. Bleher, E. Ott, C. Grebogi, Phys. Rev. Lett. **63**, 919 (1989).

48) J. E. Bayfield and P. M. Koch, Phys. Rev. Lett. **33**, 258 (1974).

49) J. E. Bayfield, L. D. Gardiner, and P. M. Koch, Phys. Rev. Lett. **39**, 76 (1977).

50) P. M. Koch, J. Phys. Coll. **43**, C2 187 (1982).

51) J. E. Bayfield and L. A. Pinnaduwage, Phys. Rev. Lett. **54**, 313 (1985).

52) E. J. Galvez, B. E. Sauer, L. Moorman, P. M. Koch, and D. Richards, Phys. Rev. Lett. **61**, 2011 (1988).

53) L. Moorman, E. J. Galvez, B. E. Sauer, A. Mortazawi-M., K. A. H. van Leeuwen, G. v. Oppen, and P. M. Koch, Phys. Rev. Lett. **61**, 771 (1988).

54) A. K. Dhar, A. M. Nagarajan, F. M. Izraelev, and R. R. Whitehead, J. Phys. **B16**, L17 (1983).

55) J. G. Leopold and D. Richards, J. Phys. **B21**, 25 (1988).

FIG. 1a

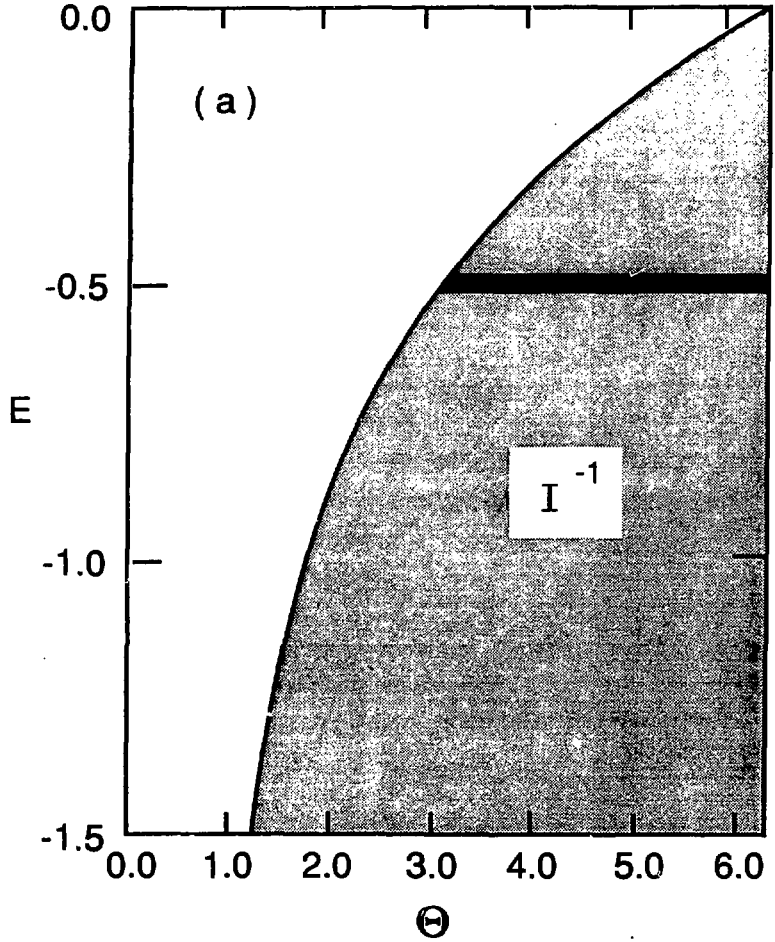

91-0888a

Fig. 16

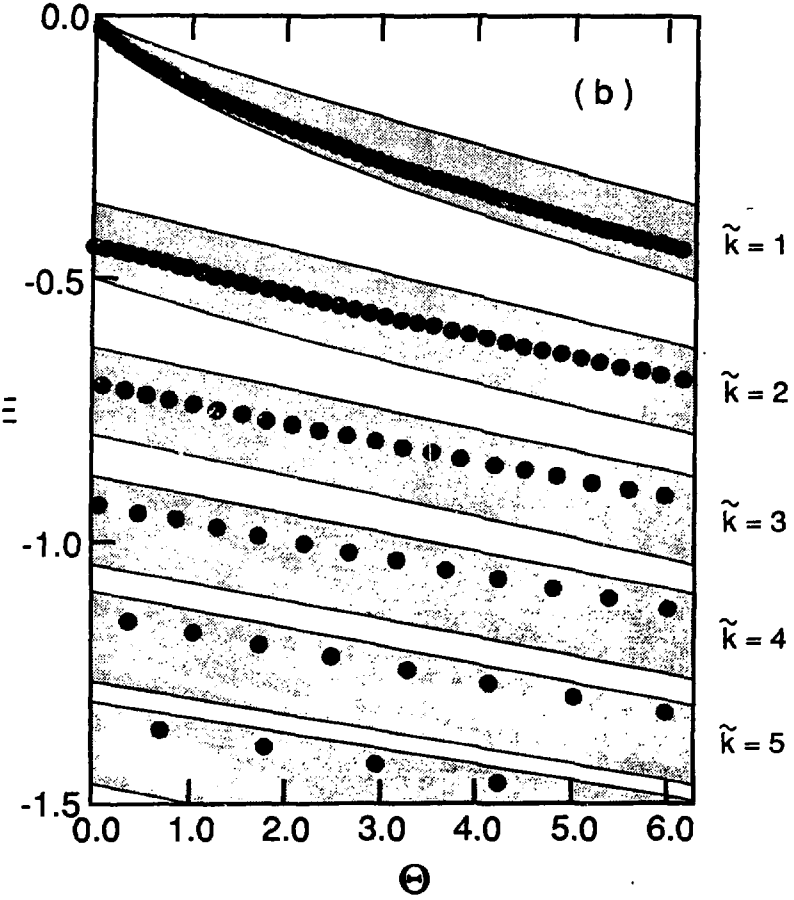

91-00838

Fig. 1c

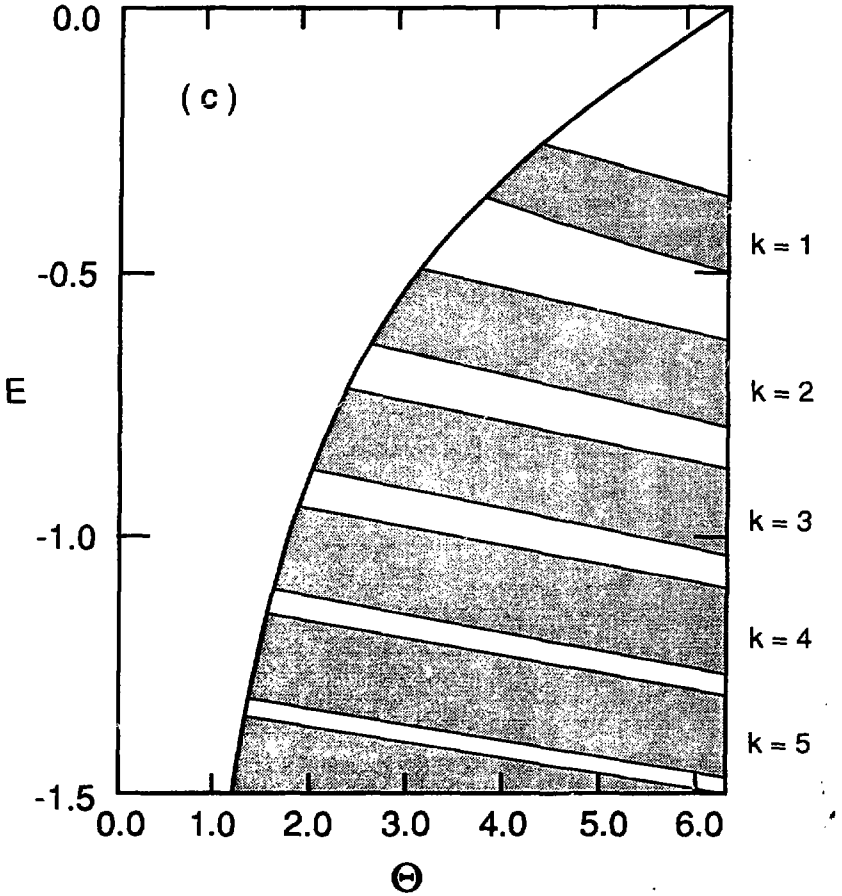

Fig. 2

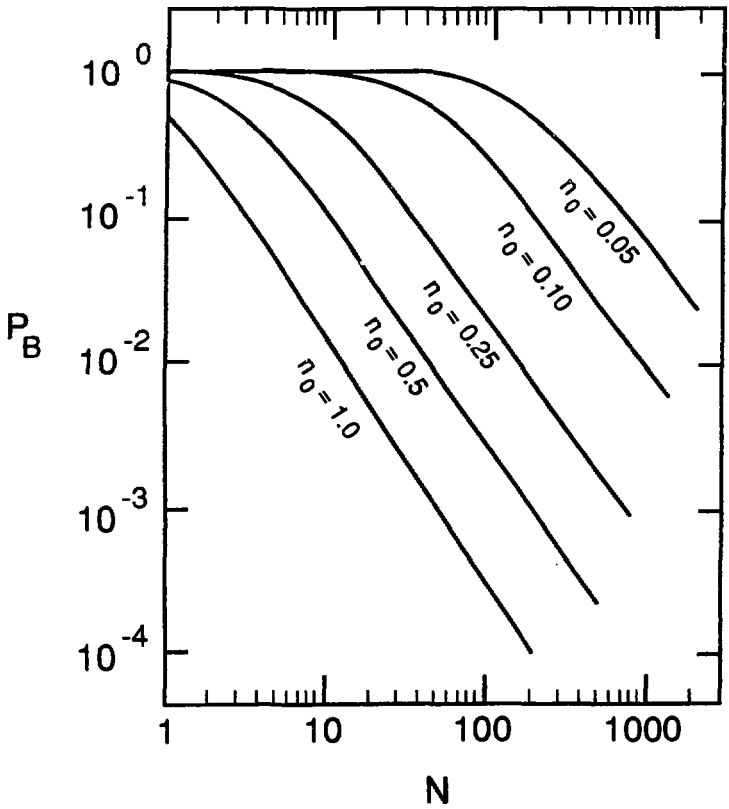

91-00830

Fig. 3

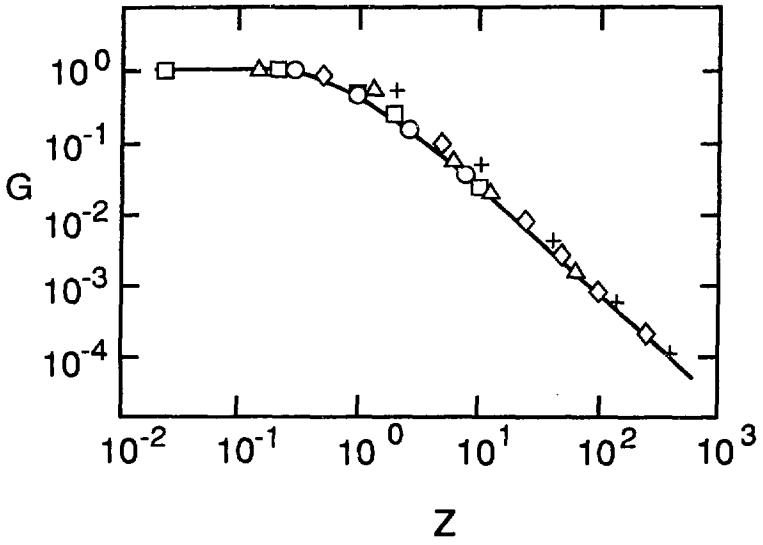

Fig. 4a

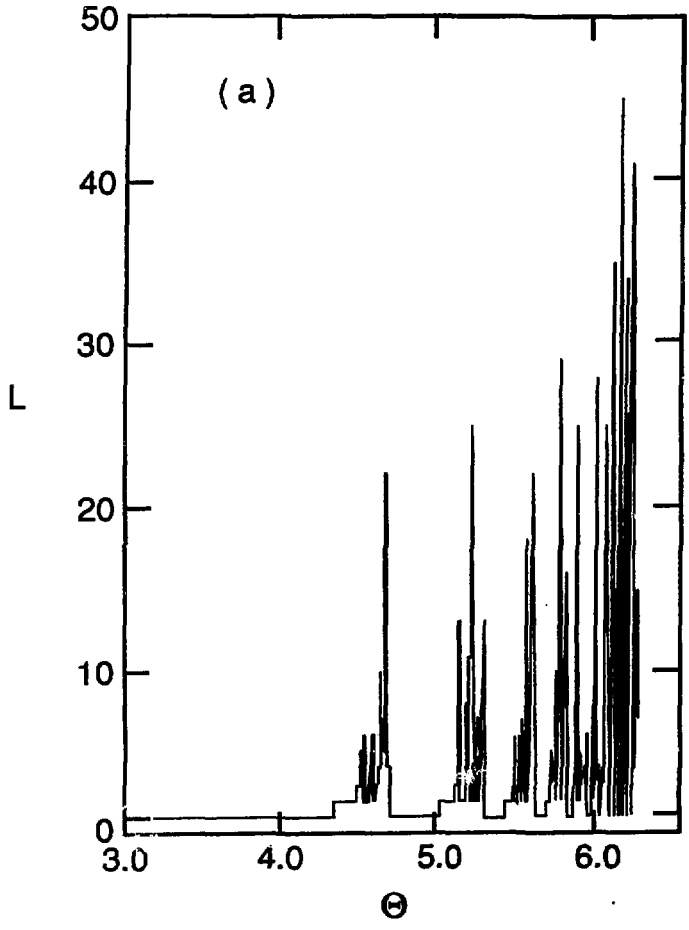

Fig. #46

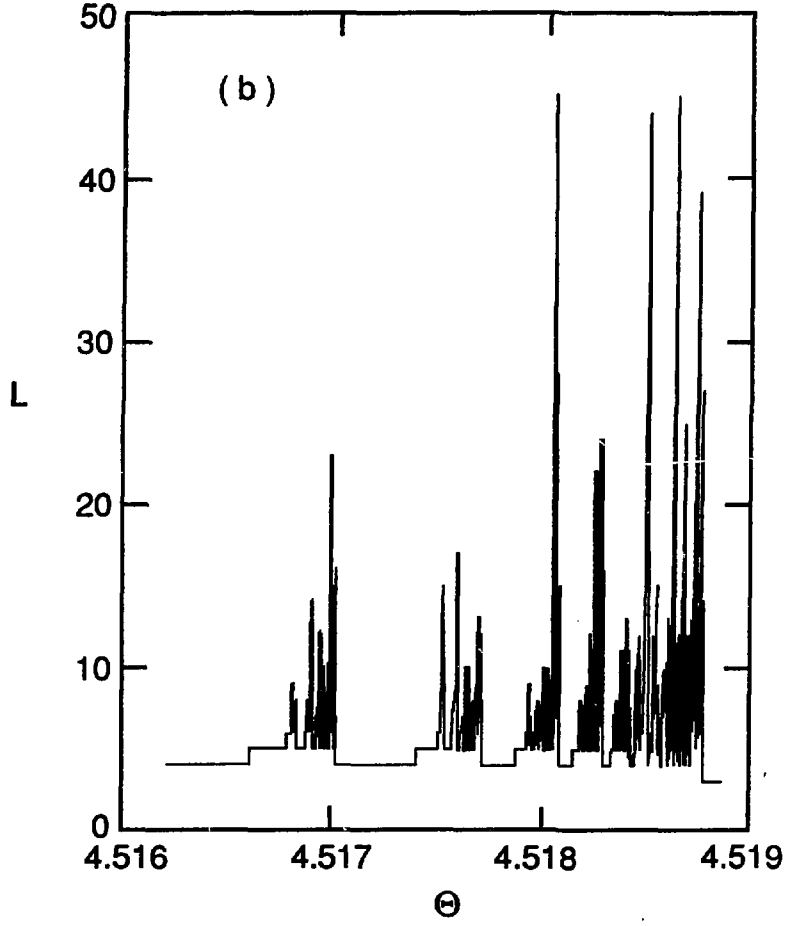

91-0083g

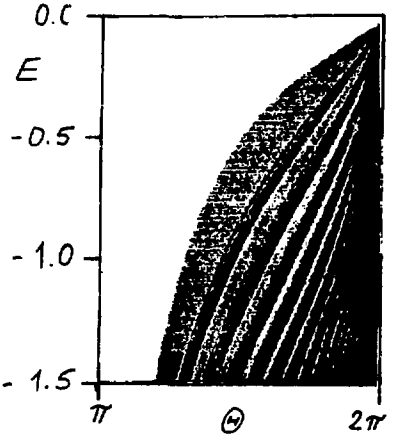

Fig. 5a

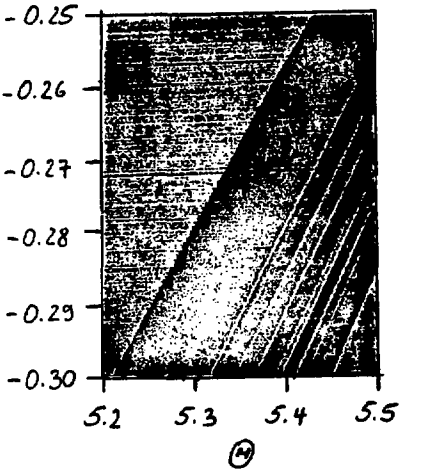

Fig. 5b

Fig. 6a

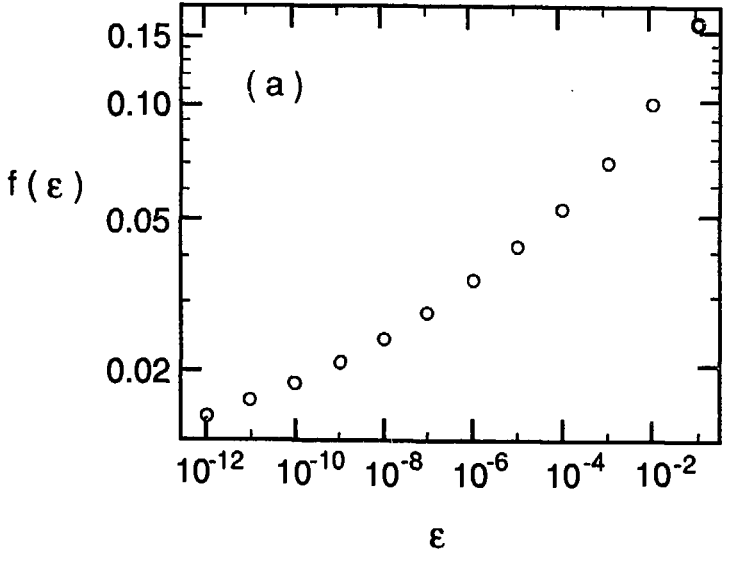

P_B

Fig. 66

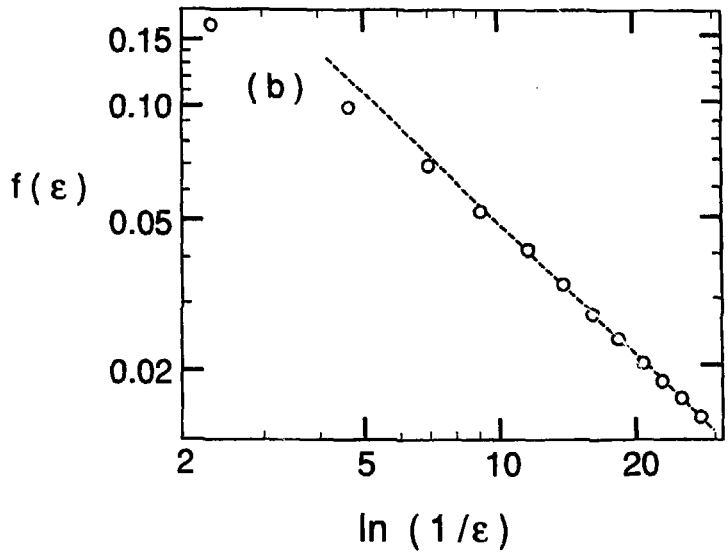

Fig. 7a

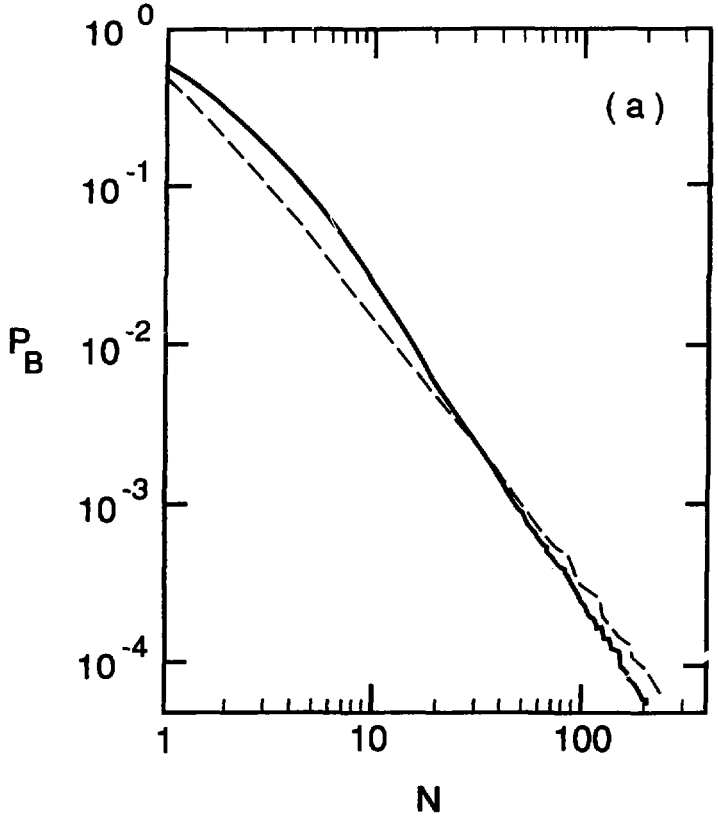

Fig. 6b

Fig. 7b

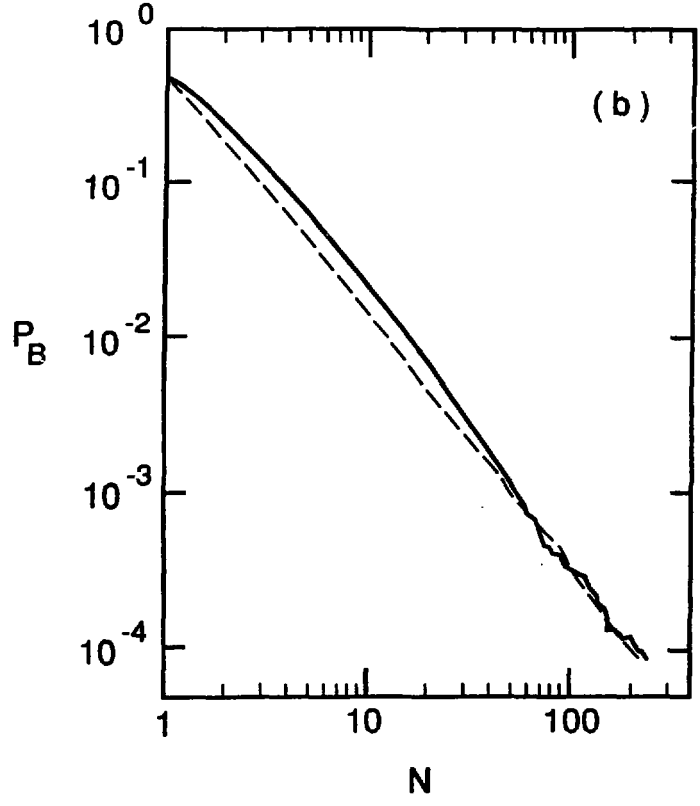

91-0083

Fig. 8

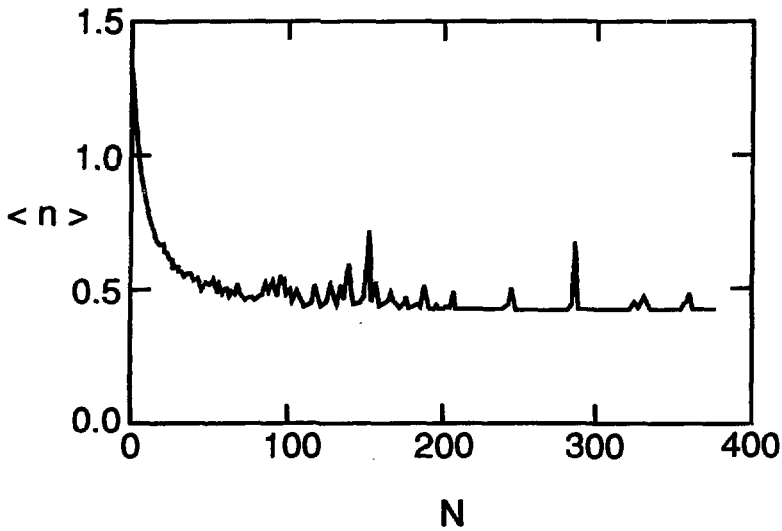

91-00838

Fig. 9

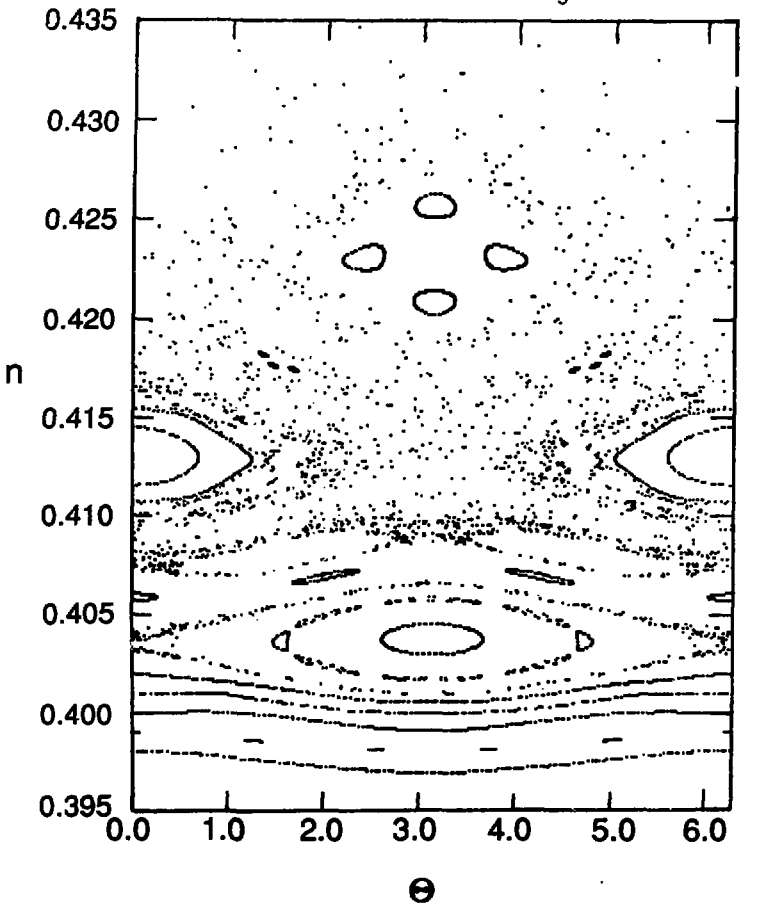

91-0068L

Fig. 10

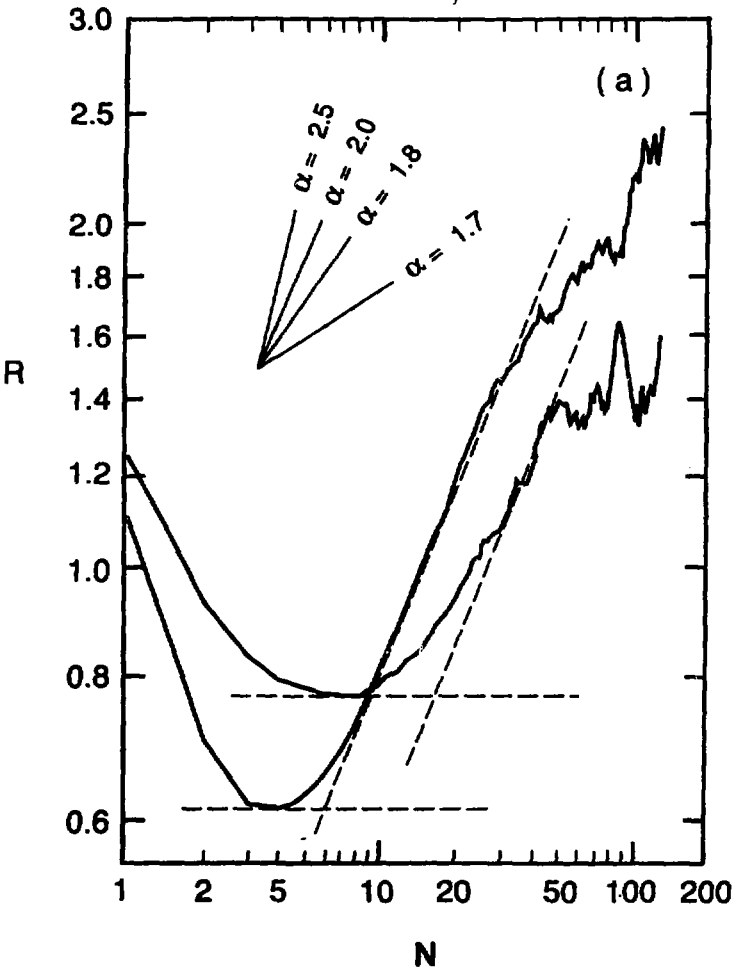
(a)
α = 2.5
α = 2.0
α = 1.8
α = 1.7
R
N
3.0
2.5
2.0
1.8
1.6
1.4
1.2
1.0
0.8
0.6
1
2
5
10
20
50
100
200

Fig 1C

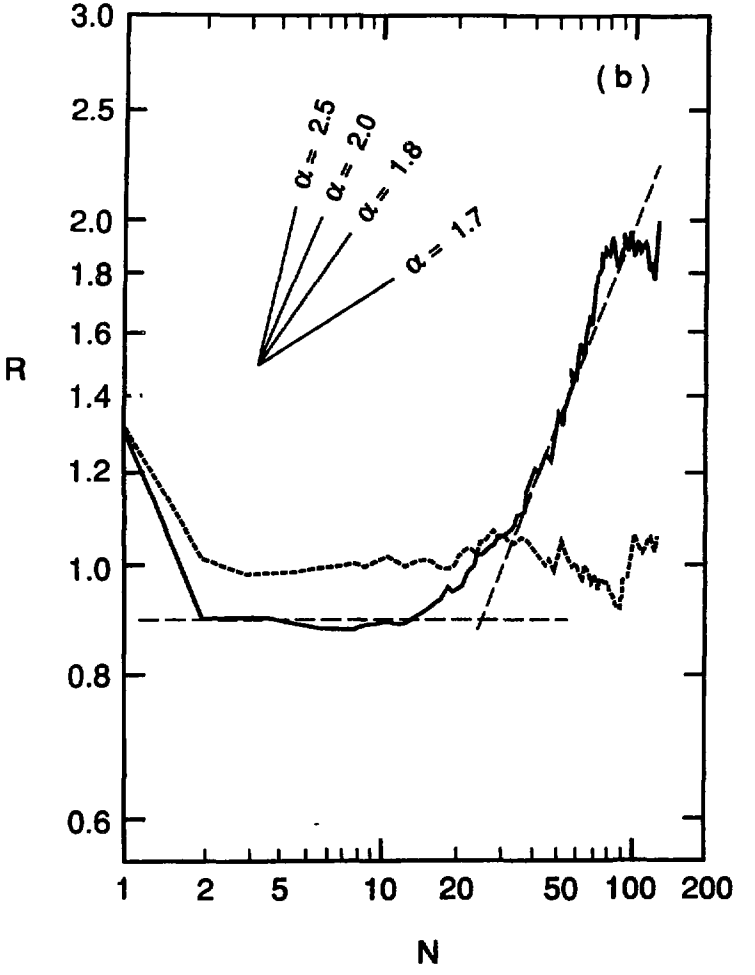
3.0
2.5
2.0
1.8
1.6
1.4
1.2
1.0
0.8
0.6
R
(b)
α = 2.5
α = 2.0
α = 1.8
α = 1.7
1
2
5
10
20
50
100
200
N